Journal of Colloid and Interface Science 685 (2025) 15–28

Contents lists available at ScienceDirect

Journal of Colloid And Interface Science

journal homepage: www.elsevier.com/locate/jcis

Chemisorption and physisorption of alcohols on iron(III) oxide-terminated surfaces from nonpolar solvents

Ibrahim E. Salama [a], Radomir I. Slavchov [b], Sorin V. Filip [c], Stuart M. Clarke [d]

[a] University of Kent, Canterbury, Kent CT2 7NZ, UK
[b] School of Engineering and Materials Science, Queen Mary University of London, Mile End Road, London E1 4NS, UK
[c] bp Applied Sciences, Technology Centre, Whitchurch Hill, Pangbourne, Berkshire RG8 7QR, UK
[d] Department of Chemistry and The Institute for Energy and Environment Flows, University of Cambridge, Lensfield Road, Cambridge CB2 1EW, UK

HIGHLIGHTS

- Alkanols chemisorb and physisorb on haematite|alkane and stainless steel|alkane.
- Adsorption data agree with a new chemisorption-physisorption adsorption model.
- Higher normal homologues chemisorb parallel to the surface, covering larger area.
- Transition from parallel chemisorbed to normal chemisorbed takes place at hexanol.
- Experimental effects of branching, solvent and temperature are well captured by the model.

GRAPHICAL ABSTRACT

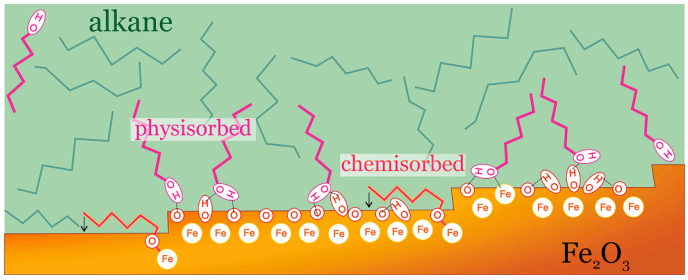

ARTICLE INFO

Keywords:
Adsorption
Alcohols
QCM
Nonaqueous
Iron oxide
XPS
Chemisorption

ABSTRACT

Hypothesis: The adsorption isotherm of alkanols at the haematite|hydrocarbon interface should reflect both chemisorption (chemically bonded fraction) and physisorption (hydrogen bonded fraction).
Experiments and model: Quartz crystal microbalance (QCM) and X-ray photoelectron spectroscopy (XPS) have been used for characterization of Fe_2O_3|hydrocarbon interfaces with absorbed alcohol. A range of Fe_2O_3-terminated surfaces, alkanols, hydrocarbons and temperatures have been investigated. A chemisorption-physisorption Langmuir model (CPL) has been developed to interpret the data.
Findings: All data show simultaneous physisorption and chemisorption of the alcohol. The CPL analysis reveals variability of the surface chemistry from one sample to another – different fractions of surface sites have been determined for Fe_2O_3-coated crystals, Fe_2O_3 powder, stainless steel-coated crystals etc. However, for a given surface, the fraction of chemisorption sites is stable – it does not change with the alcohol, and changes only slightly with the solvent. The physisorbed alcohol molecules assume configuration normal to the surface, while the chemisorbed molecules assume configuration that is either parallel (high homologues) or normal (low homologues). A transition from normal to parallel orientation has been observed at hexyl. The effects from branching of the alcohol are captured well by CPL. The temperature has been shown to alter both the strength of the physisorption and the fraction of available chemisorption sites.

E-mail addresses: i.salama@kent.ac.uk (I.E. Salama), r.slavchov@qmul.ac.uk (R.I. Slavchov).

https://doi.org/10.1016/j.jcis.2025.01.086
Received 10 October 2024; Received in revised form 10 January 2025; Accepted 11 January 2025
Available online 16 January 2025

1. Introduction

Alcohols and their derivatives are a common component of natural oils and hydrocarbons widespread in technology. A range of alkanols is currently used in biofuel blends, especially in gasoline [1–4] but also in biodiesel [5,6]. Moreover, alcohols are sometimes used as fuel additives – friction modifiers and active de-icing additives [7]. Some systems employ alkanols in the form of metal alkoxide, such as $Al_2(OC_nH_{2n+1})_3$, as 'deposit modifiers' in gasoline [8] – they are thought to become part of the deposit and beneficially alter its structure. Even when no alcohols are intentionally added to an engine fuel or lubricant oil, they are still often present at a significant concentration, due to the inevitable low-temperature oxidation of the hydrocarbons, especially in the presence of nitrogen oxides [9]. It is therefore important to understand the interaction of the alcohols with the metal|oil interface, in particular with haematite-terminated surfaces, which represent the exposed surfaces of cast iron and steel.

The adsorption on metal oxides of polar molecules from a solution in nonpolar solvents, like alcohols from oil [10–14], is a difficult problem to study. The main complications, among others, are:

(i) The variability of the surface. In most cases, a variety of different crystal faces are exposed to the liquid phase, and possibly different terminations of the same face [15–18]. There may be different levels of hydroxylation [15,19,20] and carboxylation [21] of the surface. The preparation method of the surface is essential [22–24]: it may expose layers lying below the top haematite layer; deposits from mineral particles will be present after abrasive polishing or sandblasting etc. Surface roughness may increase significantly the available area and may trigger capillary condensation and adsorption hysteresis [25]; roughening also seems to have a direct effect on the fractions of adsorption sites [26]. Surface defects such as steps may serve as adsorption sites [16]. These effects can result in limited reproducibility of the adsorption data depending on the history of the surface [22,26].

(ii) Trace impurities. The sample solutions and the ambient atmosphere contain components which chemisorb at haematite. The water content is a significant factor, even for relatively dry hydrocarbons in the 10–50 mM range [27]. Chemisorbed organic impurities are commonly found at significant surface concentrations [23] and are so difficult to remove from metal oxide surfaces that their C 1s signal in the X-ray photoelectron spectra is conventionally used for calibration (i.e. binding energies are reported not as absolute values but relative to the sp^3 nonoxidized carbon signal at 284.8 eV [28]).

(iii) Chemical reactions at the surface can be important. For example, redox processes convert the alkanol to alkoxides; low-temperature oxidation produces aldehyde and ketone [29] etc. This reactivity may cause corrosion and accumulation of deposits [30].

(iv) Competitive adsorption with the solvent [31,32].

(v) Association of the alcohol in the solution, homo- (with itself) [33] or hetero- (e.g., with water and peroxides present as impurities) [27].

Here, we present a fundamental study of the surface behaviour of alkanols, as arguably the simplest polar organic species that adsorb at the Fe_2O_3|hydrocarbon phase boundary. We have attempted to provide a mechanistic understanding for the effects of the structure of the metal|oil interface and the alcohol on the parameters of the adsorption isotherm.

2. Materials and methods

2.1. Materials

We studied adsorption of the following alkanols: ethanol (≥99.8 % purity), hexan–1–ol (anhydrous ≥ 99 %), hexan-2-ol (≥99 %), hexan-3-ol (≥97 %), dodecan-1-ol (≥98 %), 2–methylpentan-2-ol (≥99 %), 2-ethylhexan-1-ol (≥99.6 %), hexadecan–1–ol (≥99 %), from Sigma-Aldrich. They were chosen so that a range of structures is covered – different hydrocarbon chain length, branching, and different positions of the –OH group (primary, secondary, and tertiary). The solvents we used were 2,2,4-trimethylpentane (isooctane, anhydrous ≥ 99.8 %), dodecane (anhydrous ≥ 99 %) and *tert*-butylbenzene (≥99 %), from Sigma-Aldrich. These three solvents represent the three most important components of fuel and lubricants (normal alkanes, isoalkanes, arenes); we chose *tert*-butylbenzene because it is resistant to autoxidation, to avoid accumulation of surface active impurities typical for arenes containing a C—H bond in α position ($C_6H_5CHR_2$). All structures are listed in the Supplementary material S1. All samples were used without further purification apart from ethanol, which was dried over molecular sieves (3 Å). Fe_2O_3 powder was obtained from Sigma Aldrich and confirmed to be α-Fe_2O_3 via powder X-ray diffraction; Brunauer-Emmett-Teller (BET) surface area was determined as 6.05 ± 0.01 $m^2 \bullet g^{-1}$ [24]. The iron(III) oxide- and stainless SS2343 steel-coated quartz crystals ($Fe_2O_3^{QC}$ and $steel^{QC}$, for short) were purchased from Biolin Scientific. SS2343 is rich in Cr (≈18 %) and Ni (≈12 % molar), and has some Mo, Si, Mn (≈1-2 % each), and C (0.05 %) [34].

2.2. Quartz crystal microbalance (QCM)

A QCM instrument with dissipation monitoring, Q–Sense E4 system, from Biolin Scientific, was used to measure the adsorption of alcohols from alkane solution onto $Fe_2O_3^{QC}$ and $steel^{QC}$. Details about the apparatus [35], the cleaning procedures done before each run, and the measurements are provided in the Supplementary material S3.

When a substance is adsorbed on the vibrating crystal, its resonant frequency decreases. If the adsorbed mass is small compared to the mass of the crystal, and is evenly distributed and rigidly attached, with no slip or deformation due to the oscillatory motion, then the decrease in frequency (Δf) is proportional to the mass adsorbed on the crystal (Δm) according to the Sauerbrey equation [36]:

$$\Delta m = -\frac{A\sqrt{\mu_q \rho_q}\Delta f}{2n_o f_0^2} = -\frac{k\Delta f}{n_o} \quad (1)$$

Here, k is a constant equal to 17.7 $ng \cdot cm^{-2} \cdot Hz^{-1}$ for a quartz crystal of surface area $A = 1$ cm^2 and fundamental frequency $f_0 = 5$ MHz; μ_q is the elastic shear modulus of quartz (2.947×10^{11} $g \cdot cm^{-1} \cdot s^{-2}$), ρ_q is quartz density (2.65 $g \cdot cm^{-3}$), and n_o is the overtone number (1,3,5…); see supporting material S1 for a list of symbols. The resonant frequency of a 5 MHz quartz crystal can be measured with a precision of about 0.1 Hz in liquids, according to the manufacturer [35]. Therefore, from Eq. (1), adsorbed masses on the nanogram scale can be measured by the QCM. The temperature of the measuring chamber, where not specified, was kept between 23 and 25 °C. The average temperature in the laboratory was about 21 °C; the average relative humidity was 45 %. The frequency shifts were measured for two different crystals running simultaneously; the shifts were converted to adsorbed mass through Eq. (1) and the results were averaged over the overtones up to $n_o = 11$.

The device measures simultaneously the variation of the dissipation energy factor, ΔD. It reflects the viscoelastic properties of the adsorbed layer. The dissipation factor D is defined as [37] $D = E_{dissipated}/2\pi E_{stored}$, where $E_{dissipated}$ is the energy dissipated per oscillation cycle, and E_{stored} is the net stored energy in the oscillating system. The more viscous the adsorbed layer is, the more energy is lost from the oscillation. Soft, dissipating films, or films made of viscoelastic fluids cannot be analysed

via the Sauerbrey equation [36], which is only applicable [38] if $\Delta D \leq 2 \times 10^{-6}$. This condition is fulfilled for all results reported below. On some occasions, in particular at alcohol concentration above 50 mM, the recorded dissipation values were found to exceed the threshold ($\Delta D > 2 \times 10^{-6}$); accordingly, the respective measured frequency shifts were not considered further.

2.3. Depletion isotherms

A few adsorption isotherms of alcohols on Fe_2O_3 powder were determined by the solution depletion method described in ref. [14], for comparison with the QCM data.

2.4. X-ray photoelectron spectroscopy (XPS)

XP spectra were recorded using a SPECS XPS system (SPECS GmbH, Berlin) at the Cavendish Laboratory in Cambridge. The spectrometer is equipped with Al Kα monochromatic source ($h\nu = 1486.6$ eV) operating at 30 W, composed of a SPECS XR50 MF X-ray gun and a μ-FOCUS 600 monochromator, and PHOIBOS 150 1D-DLD analyser. All binding energy values reported in this paper are relative to the Fermi level. All spectra were calibrated against the peak for nonoxidized sp^3 carbon in adventitious organic impurities at 284.8 eV [28] and corrected using a Shirley background. The XPS CASA program (Casa Software Ltd., Cheshire, UK) was used to deconvolute the data. Analysis was made of the $Fe_2O_3^{QC}$ and $steel^{QC}$ surfaces before contact with the oil phase (pristine surfaces) and after contact with hexanol solution in alkane (i.e. surfaces with pre-adsorbed alcohol and possibly solvent molecules). The XPS measurements were taken under vacuum where weakly bound material is expected to evaporate; only strongly adhering molecules remain at the surface. This certainly includes chemisorbed (i.e. chemically bonded) alcohol; moreover, we expect that some strongly bound physisorbed alkanol (e.g., double hydrogen bonded) also remains at the surface. Indeed, both chemisorbed and physisorbed water are detectable on iron oxides even after prolonged degassing [39,40].

3. Results and interpretation

3.1. XPS of the solid surfaces

The XP survey spectra of both $Fe_2O_3^{QC}$ and $steel^{QC}$ in Fig. 1(a) show peaks at binding energies of ~ 710, 530, 285, 95, 55, and 20 eV, attributable to photoemission from core levels of Fe 2p, O 1s, C 1s, Fe 3s, Fe 3p, and O 2s/C 2s photoelectrons, respectively. The broad peaks centred at 974, 894, 847 and 785 eV can be assigned to Auger transitions of Fe and O. Stainless steel SS2343 contains more elements. The XPS signal from these elements is weak: there are Cr 2p peaks at ~ 575 eV, but the Ni region at 855 eV (strongly overlapping with Fe_{LMM}) does not imply significant concentration of Ni on the surface, and the same can be said for Mo, based on the region ~ 230 eV. Ni and Mo indeed have little affinity to the surface of steel under oxidizing conditions [41]. Mn and Si may sometimes be dominant components in the outermost oxide layers, depending on the history of the probe [41,42]; in Fig. 1(a), weak Mn 2p peaks can be seen around 640 eV, but the Si region (100 eV) differs little for $Fe_2O_3^{QC}$ and $steel^{QC}$. Thus, the surfaces of our SS2343- and Fe_2O_3-coated plates show broadly similar surface chemistry, dominated by Fe_2O_3, with some Cr, and perhaps traces of Ni and Mn on the $steel^{QC}$ surface.

The high-resolution **Fe 2p spectrum of pristine Fe_2O_3**, Fig. 1(b), exhibits two distinct signals, Fe $2p_{3/2}$ at ~ 710.7 eV and Fe $2p_{1/2}$ at ~ 724.3 eV, with a satellite located at 718.8 eV, which is a feature of α-Fe_2O_3 [43,44,45]. The minimum number of peaks sufficient to deconvolute the Fe $2p_{3/2}$ signal is three – these are found at binding energies of 709.5, 710.7 and 712.8 eV, and can be assigned to Fe^{2+}(**Fe**O-type), Fe^{3+}(**Fe**$_2$O$_3$-type) and Fe^{3+}(**Fe**O-OH-type), respectively. The Fe^{2+} responsible for the 'pre-peak' at 709.5 eV is usually assumed to be produced during the surface preparation [46]. The $2p_{3/2}$ level is actually a triplet [46], so this deconvolution is approximate.

The respective high-resolution **Fe 2p region of pristine $steel^{QC}$** surface is shown in Fig. 1(c). The deconvolution of this signal requires at least 4 peaks; these may be assigned [43,44,46] to neutral iron Fe^0 at 707.1 eV, Fe^{2+} at 709.8 eV, Fe^{3+}(**Fe**$_2$O$_3$) at 710.7 eV, and Fe^{3+}(**Fe**O-OH) at 712.9 eV. The similarity of the spectra of stainless steel and Fe_2O_3 shows that $steel^{QC}$ is haematite-terminated, as expected in the presence of oxygen [47,23]. The signals assigned to Fe^0 and Fe^{2+} may come from

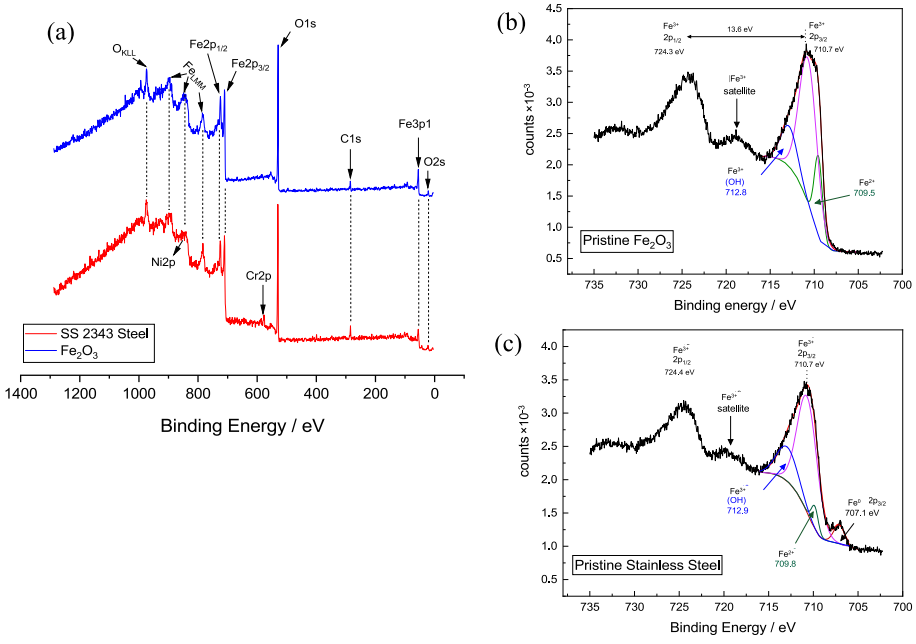

Fig. 1. (a) XP survey spectra of as received iron oxide- and stainless steel-coated crystals ($Fe_2O_3^{QC}$ and $steel^{QC}$). Fe 2p high resolution peaks for (b) iron(III) oxide and (c) stainless steel, with deconvolution.

layers of $FeCr_2O_4$, Fe_3O_4 and iron lying below the top layer of Fe_2O_3; from cementite; or from defects made during the preparation of the surface. A similar high-resolution **Cr 2p spectrum** was recorded for the surface of steel^{QC} and deconvoluted to a main Cr^{3+} feature at 576.5 eV, another for **Cr**–OH at 579.3 eV, and a narrow peak at 574.2 eV for metallic chromium [48,49]. The data agree with a typical oxidized 18 % chromium steel surface, where the top layer of the iron surface, Fe_2O_3, is substituted with a solid mixture $Fe_2O_3 + Cr_2O_3$ (Cr-depleted compared to the base alloy), and the second layer of Fe_3O_4 is substituted by partially miscible spinnels ($FeCr_2O_4$ and Fe_3O_4 with some Ni^{2+}) [50,47].

Hence, the surface of stainless steel is similar to that of haematite in terms of main chemical functionality (featuring partial hydroxylation) but differs to some extent in surface concentration of functional chemical groups and, moreover, has more admixtures and defects, as can be expected.

3.2. XPS of $Fe_2O_3^{QC}$ after adsorption of hexanol – Fe 2p region

Fig. 2(a) shows the high-resolution spectra of the pristine Fe_2O_3-coated crystals, with no hexanol adsorbed. After adsorption from 10 mM hexanol in dodecane on $Fe_2O_3^{QC}$, we observed a decrease in intensity of the peaks of Fe $2p_{1/2}$ at 724.3 eV and Fe $2p_{3/2}$ at 710.7 eV, Fig. 2(b). Moreover, the peak at 710.7 eV shifted to lower binding energy of 710.1 eV. A further increase of concentration to 30 mM hexanol leads to a further decrease of the intensities of Fe $2p_{3/2}$ and Fe $2p_{1/2}$, Fig. 2(c), but without further shift. The FeO-OH peak at 712.9 eV is not shifted, but its intensity changes in parallel to the main Fe_2O_3 peak.

The decrease in intensity of the iron signals is due to screening from the layer of hexanol adsorbed at the surface. The shift may be due to formation of FeO-OC_6H_{13} (hexanol chemisorbed as hexoxide). Chemisorption is approximately concentration independent [31,51]; therefore, the difference between the spectra at 10 mM and 30 mM shows that a fraction of the physisorbed hexanol remains at the surface, surviving the drying process before measurement and the vacuum in the XPS chamber. Similar behaviour has been reported for adsorption of water vapour [39].

An attempt has been made to desorb the alcohol by sonication in pure isooctane of the $Fe_2O_3^{QC}$ surface with hexanol pre-adsorbed from 30 mM solution. This did not remove the adsorbed hexanol molecules completely, as inferred from Fig. 2(d). The XPS peak intensities in Fig. 2 suggest a level of adsorption after the washing the 30 mM probe similar to that of the unwashed 10 mM probe. A possible explanation is that, at 10 mM, most of the sites that allow chemisorption are already occupied but without significant physisorption, and a further increase to 30 mM contributes to the physisorption of alcohol only. The washing process leaves the chemisorbed molecules at the surface; in contrast, the complete cleaning procedure described in the Supplement S3 (involving high-temperature treatment in an oven) does return the surface to the initial pristine state.

3.3. O 1s core level

The high-resolution XP spectrum of pristine $Fe_2O_3^{QC}$ surface exhibits an asymmetric O 1s peak. It was deconvoluted into two peaks: one at 529.6 eV, associated with the lattice oxygen ($Fe_2\mathbf{O}_3$, see Fig. S1(a) in S2), and a second at 531.1 eV, attributed to surface hydroxyl (FeO – **O**H) groups, in agreement with literature [15,52,53]. Organic > C═O from adventitious impurities and metal carbonates likely contribute to the latter signal.

Fig. S1(b) in S2 shows the O 1s core-level spectrum from $Fe_2O_3^{QC}$ that had been in contact with 10 or 30 mM hexanol solution in dodecane. In this case, the high-resolution XP spectrum can be deconvoluted into four peaks. In the presence of hexanol, the main peak at 531.1 eV is probably a combination of FeO-**O**H and oxygen in iron(III) hexoxide (FeO-**O**C,

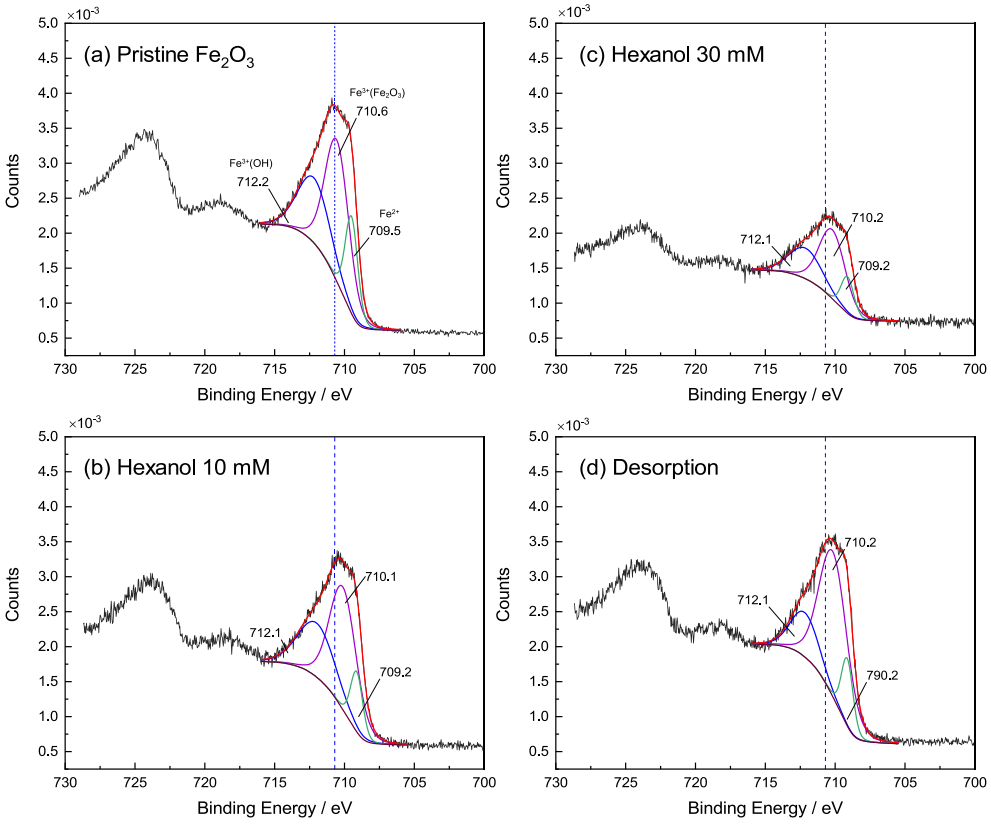

Fig. 2. Fe 2p core-level photoelectron spectra of (a) pristine Fe_2O_3; (b) after adsorption of hexanol (10 mM); (c) after adsorption of hexanol (30 mM), and (d) after desorption from the sample from (c).

formed by dissociative adsorption of alcohol [54–57]). The peak at 533 eV is the physisorbed C_6H_{13}**O**H, and possibly water [58]; its presence again confirms that the vacuum in the XPS chamber does not remove the physisorbed hexanol completely. The last peak at 536 eV is difficult to assign, but the large shift may correspond to a peroxide bond. Peroxides are the primary products of oxidation of organics [59,9], and the formation of oxidation products resulting from the X-rays exposure of the alcohols is well-documented; iron catalysis may contribute to the rate of oxidation [59]; another possible explanation is free water released in the gas phase [15].

Increasing the hexanol concentration C from 0 to 10 mM and further to 30 mM decreases the intensity of the main Fe_2**O**$_3$ peak due to screening of the signal by the adsorbed layer of hexanol, similar to the drop in the area of the **Fe**$_2$O$_3$ peaks in Fig. 2. Importantly, the intensity of the second peak at 531.1 eV increases; this is evidence for alkoxide formation (i.e. this is a compound signal from screened FeO-**O**H and newly appearing FeO-**O**C).

Sonicating $Fe_2O_3^{QC}$ with pre-adsorbed hexanol (30 mM probe) in pure alkane desorbed all the physisorbed alcohol and also the hypothetical oxidation products – the peaks at 533 and 536 eV disappear. Moreover, the main two peaks in the spectrum return to their 10 mM values. The intensity of the 531.1 eV peak drops after washing but remains higher than that of the pristine haematite; this means that some, but not all, chemisorbed molecules are irreversibly bound to the surface. The full cleaning procedure (see S3) results in peaks going back to the intensities of pristine $Fe_2O_3^{QC}$.

3.4. C 1s core level

The high-resolution C 1s XPS signal for pristine iron oxide surface is reported in Fig. S2(a) in S2. The signal can be deconvoluted into three peaks that we assigned to sp^3 chain carbon [60] (C—**C**—C and C—**C**—H, 284.8 eV), sp^3 carbon adjacent to oxygen [60–63] (C—**C**—O, ~286 eV), and carbonates and organic sp^2 carbon in a carbonyl group [60] (>**C**═O, ~288–289 eV). This last C 1s signal is a consequence of adventitious CO_2 and organic contamination deposited as a result of the exposure to air [64]. The first peak was used as reference for the entire spectrum and was set to [28] 284.8 eV. The observed binding energy separations from the main carbon peak agree with published values [65–68].

The adsorption of hexanol from 10 mM dodecane solution onto $Fe_2O_3^{QC}$ resulted in increased intensity of the three main carbon peaks, as shown in Fig. S2(b and c). These three peaks changed little upon further increase in concentration to 30 mM or washing. The increase in the >**C**═O peak at 288 eV could be due to oxidation of the adsorbed layer to various products under the action of the X-rays, O_2 and iron catalysis; it is possible that the hexoxide carbon (C_5H_{12}**C**H_2O–Fe) contributes to this peak. Moreover, two new peaks at 293 and 295–296 eV evolved on the high-energy side of the C—C component. These disappear after sonication in isooctane. The assignments of these two peaks were not conclusive.

3.5. Comparison with previous results

There are several spectroscopic studies in the literature that can be compared to ours. Kataby et al. [55] studied the adsorption of octan-1-ol, dodecan-1-ol and tridecan-1-ol from concentrated ethanol solutions on iron nanoparticles using XPS and Fourier transform infrared spectroscopy (FTIR) at room temperature. They reported the Fe $2p_{3/2}$ and O 1s spectra of pristine iron and alcohol-coated iron surfaces; the iron appears to be Fe_2O_3-terminated, and the solvent used (ethanol) is unlikely to allow any observable physisorption of the solutes. The FTIR spectrum of the adsorbed alcohol onto iron oxide nanoparticles showed that alcohol (either solute or solvent) is bonded to the surface of the iron nanoparticles mostly through FeO-OC bonds [55]. They also found that the O—H stretching vibration of the alcohol at 3288 cm^{-1} disappears upon adsorption, confirming the formation of a chemical bond between the alcohol and iron. Thus, in contrast to our systems, physisorption of the alcohol was negligible for the solutions they studied, probably because the ethanol solvent dominated the physisorbed layer but evaporated before the spectrum was taken.

Busca [69] reported IR results that show both physisorbed and chemisorbed fractions of adsorbed isopropanol vapours on haematite. In contact with the alcohol vapour, the physisorbed fraction gives the stronger signal, but after degassing, only the chemisorbed fraction remains at the surface. The chemisorbed isopropanol appears to be in the form of isopropoxide, FeO-O-i-Pro, formed by dehydration from FeO-OH and i-ProOH, or possibly by addition to two adjacent oxygens (Fe_2O_3 + i-ProOH → Fe_2O(OH)-O-i-Pro). Methanol and ethanol were found to behave similarly [29,69].

The XPS binding energy shift in Fe 2p and O 1s has been reported [70] for the adsorption of aqueous phenol (at varying pH) on iron oxide nanoparticles (probably haematite-terminated magnetite) at 30 °C. The oven-dried samples showed little, if any, phenol adsorption; the data may be complicated by a corrosion process.

3.6. Adsorption model

The XPS results show that at least two distinct populations of alcohol molecules exist at the surface: chemisorbed and physisorbed. The adsorption isotherm has to reflect this. Moreover, the two populations can assume different configuration at the surface. The data reported below indicate that long chemisorbed alcohols tend to lie parallel to the surface; this is because the chain orientation is restricted by a metal alkoxide bond of fixed geometry (FeO–OC_nH_{2n+1}), and the shorter chemical bond facilitates stronger chain-surface interaction. By contrast, a physisorbed alcohol molecule is linked to the surface by longer and less specific hydrogen bonds and, therefore, can assume a range of configurations; in a dense monolayer of physisorbed alcohol, the hydrocarbon chains should approach approximately normal orientation with respect to the surface.

Let the population of chemisorption sites be of surface density Γ_c (number per unit area), and let these be completely occupied at any nonzero concentration of alkanol, as typical for chemisorption [31]. Let the density of physisorption sites be Γ_p. For simplicity, we assume that the areas per physi- and chemisorption site are both equal to a_p. The value of a_p is perhaps about 15 $Å^2$ per site (this is the area per oxygen atom at the {001} face of haematite [71]). As a further approximation, we assume that the cross-sectional area of a physisorbed alcohol molecule standing upright is again equal to a_p – the crystallographic cross-sectional area of normal alcohols is ~ 18 $Å^2$ [72], close to the site area.

The area a_c covered by a chemisorbed molecule may be larger than a_p if the axis of the hydrocarbon chain of the chemisorbed molecule is inclined at a small angle to the surface, such that a larger projected area is covered compared to the upright physisorbed species. Thus, a chemisorbed molecule covers simultaneously the chemisorption site to which it is linked and $(a_c–a_p)/a_p$ adjacent sites. Of these, some are chemisorption and others are physisorption sites, of amount set by their mean fraction for the surface. If the fraction of chemisorption sites is $x_c = \Gamma_c/(\Gamma_c + \Gamma_p) = a_p\Gamma_c$, then each chemisorbed molecule covers N_c chemisorption sites, where:

$$N_c = 1 + \frac{a_c - a_p}{a_p} x_c = 1 + (a_c - a_p)\Gamma_c \quad (2)$$

For N_c chemisorption sites bound by each chemisorbed molecule, the surface concentration $\Gamma_{chemisorption}$ of chemisorbed alcohol is by a factor of N_c smaller than the number Γ_c of available chemisorption sites:

$$\Gamma_{chemisorption} = \frac{\Gamma_c}{N_c} = \frac{x_c}{a_p + (a_c - a_p)x_c} \quad (3)$$

This formula predicts that the chemisorption decreases as the hydro-

carbon chain length of the alkanol increases – the larger area a_c occupied by a longer alkanol covers multiple chemisorption sites, preventing them from binding the head group of another molecule. The minimum value of a_c is a_p (one site covered) and it corresponds to $\Gamma_{chemisorption} = \Gamma_c$ (all chemisorption sites occupied). In the other limit of very large a_c, complete coverage of the surface is approached by the chemisorbed molecules alone ($\Gamma_{chemisorption} = 1/a_c \ll \Gamma_c$), with no available sites for physisorption.

The physisorption takes place on the fraction $1–a_c\Gamma_{chemisorption}$ of the surface area not occupied by chemisorbed molecules. We assume a simple Langmuir isotherm holds for the physisorbed alcohol:

$$\Gamma_{physisorption} = \frac{K_a \gamma C}{1 + a_p K_a \gamma C}\left(1 - a_c \Gamma_{chemisorption}\right) \tag{4}$$

Here, the *physisorption constant* K_a is defined in units [m] (compared to Langmuir's constant $K = a_p K_a$ in units m^3 or m^3/mol); γ is the activity coefficient of the alcohol in the bulk alkane solution.

QCM measures the QC mass change upon exchange of pure solvent with a solution. Hence, there may be a contribution from the detachment of solvent as the additive adsorbs, depending on the strength of binding of the solvent to the substratum. If the solvent binding is weak (more precisely, if the binding of solvent to pristine surface and to surface with alcohol layer do not differ significantly), then additive adsorption alone will be followed by the QCM. In this case, the alcohol adsorption measured by QCM corresponds to $\Gamma = \Gamma_{chemisorption} + \Gamma_{physisorption}$, or from Eqs. (3)&(4):

$$\Gamma = \frac{x_c + a_p K_a \gamma C}{\left[a_p + (a_c - a_p)x_c\right](1 + a_p K_a \gamma C)} \tag{5}$$

We refer to Eq. (5) as the *chemisorption-physisorption Langmuir model* (CPL). It involves four adsorption parameters. It can be assumed that the first of them, the fraction x_c of chemisorption sites, depends on the nature of the surface, but not on the structure of the adsorbed alcohol. For normal alcohols, the area a_p is expected to have value close to their crystallographic cross-sectional area. The area per chemisorbed alcohol a_c is at least equal to a_p and should not exceed by much $(n + 1) \times a_p$ (corresponding to the assumption that each CH_2 group covers one site for molecule parallel to the surface). Finally, the physisorption constant, K_a, is related to the free energy of formation of one or two hydrogen bonds and the loss of transitional degrees of freedom upon adsorption. K_a can be expected to depend strongly on the degree of hydroxylation, the temperature, the crystal face, and weakly on the nature of the solvent and the hydrocarbon chain of the alkanol.

Alkanols are known to associate in alkanes and hence the activity coefficient γ is appreciably smaller than 1 already at $C = 20$ mM [33]. The association is represented by an equilibrium of monomer and associates. The extent of association increases with increasing concentration and depends on the association equilibrium constant for the studied system. We calculated the activity coefficient by solving the approximate monomer-tetramer equation $C = \gamma C + 4K_4(\gamma C)^4$ for γ at each experimental concentration; here, $K_4 = 780\ M^{-3}$ [33] is the tetramerization constant of the alcohol in the oil phase (see S5). The association is driven by the polar head groups and hence we used the same value for all alcohols in this work. Since K_4 does depend to some extent on the structure of the alcohol and the solvent, the computed γ values are approximate. Nevertheless, the activity correction is rarely important for the concentration range we study, because the data that are affected fall in the plateau region of the isotherm, where the correction produces a shift in the direction of the x-axis that has almost no effect on our conclusions.

For comparison, McCafferty and Zettlemoyer successfully used a similar model for water vapour adsorbing on haematite [73]; physisorbed water, however, forms a multilayer, so they used the BET isotherm for $\Gamma_{physisorption}$ instead of Langmuir's. The areas a_c for hydroxyl and a_p for H_2O are approximately equal, and McCafferty and Zettlemoyer were able to control the initial hydroxylation (i.e. x_c) of the fresh surface via the outgassing temperature. Most other studies in the literature ignore the chemisorption. For example, Lee and Staehle tried BET without chemisorption to find that it "consistently underestimates amounts of adsorbed water at low and intermediate relative humidity" [74]. They had better success with the Frenkel model [75,76], which qualitatively resembles a chemisorption-physisorption isotherm at low concentrations (but this model was originally developed for multilayer physisorption at very high coverages only).

3.7. Adsorption data and adsorption parameters

3.7.1. Effect of hydrophobic chain length

We first investigated the effect of the alcohol chain length on the amount of n-$C_nH_{2n+1}OH$ (n = 2,6,12,16) adsorbed from dodecane on $Fe_2O_3^{QC}$, Fig. 3(a). We limited ourselves to concentration below 20 mM (30 mM for ethanol), as, above that, the viscosity of the solution changes and Sauerbrey's equation is not applicable. In the range considered, ethanol and hexanol follow L-type of adsorption [77], with a plateau at $C > 1$–5 mM. The isotherms of dodecanol and hexadecanol appear to be more complex. The adsorption at a given concentration decreases with the increase in length of the hydrocarbon chain ($\Gamma_{ethanol} > \Gamma_{hexanol} > \Gamma_{dodecanol} > \Gamma_{hexadecanol}$). A similar trend was reported for adsorption of short chained alcohols from heptane on Fe_2O_3 powder [13], from decane on kaolinite [78], and for $n = 2$, 8 and 12 from p-xylene and n-heptane on rutile [79].

We analysed the data by comparing them with the CPL model (5). To reduce the number of fitting parameters, we assumed that the area a_p (cross-section of physisorbed molecule & area per site) is independent of n; moreover, all $Fe_2O_3^{QC}$ plates were assumed to have the same surface chemistry, so the fraction x_c of chemisorption sites is the same for all four data sets. The data for the four alcohols (n = 2,6,12,16) were fitted simultaneously with the remaining 10 parameters (one x_c, one a_p, four a_c and four K_a, i.e. 2.5 free parameters per isotherm of each alcohol), by optimizing the following merit function:

$$\delta_\Gamma^2 = \sum_n \sum_i \left[\Gamma(C_{n,i}; x_c, a_{c,n}, a_p, K_{a,n}) - \Gamma_{n,i}\right]^2 / (N - 10) \tag{6}$$

Here, $\{C_{n,i}, \Gamma_{n,i}\}$ is the i^{th} experimental data point for the n^{th} alcohol, i.e. we fit a three-column table (with values of set n and C and measured Γ)

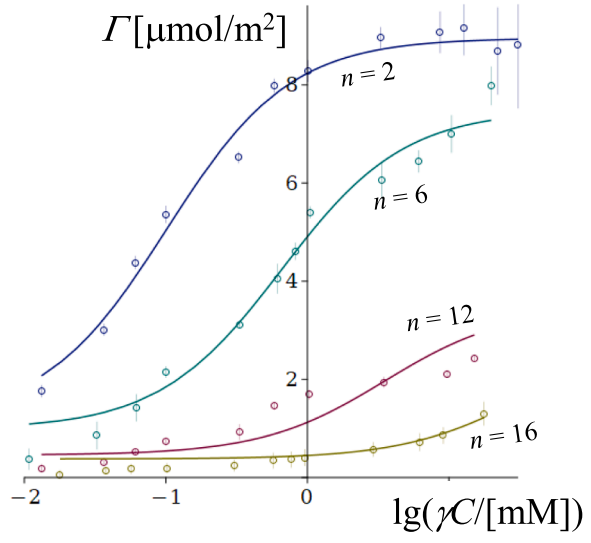

Fig. 3. Adsorption Γ vs activity γC of $C_nH_{2n+1}OH$ for n = 2,6,12,16 adsorbed on Fe_2O_3-coated quartz crystal ($Fe_2O_3^{QC}$) from dodecane at 23 °C. Lines are the CPL model (5), with the parameters in Table 1.

with a theoretical surface $\Gamma(C,n)$.

The results are presented in Fig. 3 and Table 1. The fitted value of the fraction of chemisorption sites is $x_c = 13$ %, i.e. one in 7–8 surface sites binds chemically the alcohols. The area a_p found from the regression is 18.5 Å^2, practically equal to the crystallographic area of solid alkanols [72], somewhat higher than the area per oxygen atom at Fe_2O_3 {001} surface (15 Å^2 [71]), but close to water's BET area per molecule on haematite (21 Å^2 [80]). The area a_c increases with n, as Fig. 4 shows; this confirms that the chemisorbed molecules have a small inclination angle with respect to the surface. Chemisorbed ethanol covers a single site (the fitted a_c was at its lowest allowed value equal to a_p); hexanol covers 2.5 sites (one occupied chemisorption site and 1.5 additional sites blocked by the hydrocarbon tail). The tails of chemisorbed dodecanol and hexadecanol appear to cover large areas, but the CPL isotherm is not very sensitive to the exact value of a_c in these cases. To avoid unphysically large areas, we set an upper limit for this parameter: $a_c = (n + 1)a_p$, and the optimization produced values of a_c at this limit for $n = 12$ and 16. Finally, the physisorption constants of the four alcohols decrease with the length of the hydrocarbon chain ($K_a = 90$, 14, 2.5 and 0.25 μm for $n = 2$, 6, 12 and 16, respectively, see Fig. S6 in S4).

To investigate further the validity of the model and the dependence of a_c and K_a on n, we analysed the data by Allen and Patel [13] for adsorption of butanol, hexanol and octanol from heptane on Fe_2O_3 powder. The adsorption Eq. (5) agrees well with their data. For this analysis, to reduce the number of fitting parameters, we set a_p equal to 18.5 Å^2, as found from our QCM measurements. The rest of the parameters were obtained from the fit. The comparison between the model and the data is shown in Fig. S5 in S4, and the parameter values are listed in Table 1. The fraction of chemisorption sites at the surface of Allen and Patel's Fe_2O_3 powder is higher than that at our Fe_2O_3-coated quartz crystal: $x_c = 22.5$ % for $Fe_2O_3^{powder}$, one in 4–5 sites (vs 13 % for $Fe_2O_3^{QC}$). The obtained areas per chemisorbed molecule follow a trend with n that agrees well with that from our own data, Fig. 4. However, the adsorption constant derived from Allen and Patel's measurements is less dependent on n than ours ($K_a = 1.2$, 2.1 and 2.2 μm for $n = 4$, 6 and 8; the dependence is plotted in Fig. S6 in S4).

The data by Nakayama and Studt [10,11] for octadecanol adsorbing on iron metal powder from hexadecane were analysed similarly (Fig. S5). The outermost layer of metallic iron is expected to be Fe_2O_3 again. The fitted values indicate fewer chemisorption sites on this surface ($x_c = 1.3$ %). As with our data for dodecanol and hexadecanol, the area per chemisorbed octadecanol is found to be at the upper allowed limit, $a_c = 19 \times a_p$. The physisorption constant is 17 μm, close to ours for hexanol, but larger than our K_a values for higher alcohols (Fig. S6).

Table 1
The parameters of the CPL model for alcohols at the alkane|haematite interface.

Alcohol	Interface	a_p [Å^2]	a_c	x_c	ln(K_a/[m])	δ_Γ[μmol/m^2] [e]
C_2H_5OH [a]	$Fe_2O_3^{QC}$| dodecane	18.55	[d] |1 × a_p	0.1315	−9.34	0.35
$C_6H_{13}OH$ [a]			2.49 × a_p		−11.20	
$C_{12}H_{25}OH$ [a]			[d] 13| × a_p		−12.88	
$C_{16}H_{33}OH$ [a]			[d] 17| × a_p		−15.18	
C_4H_9OH [b]	$Fe_2O_3^{powder}$| heptane	[d] | 18.55|	1.53 × a_p	0.225	−13.60	0.09
$C_6H_{13}OH$ [b]			2.76 × a_p		−13.06	
$C_8H_{17}OH$ [b]			7.70 × a_p		−13.02	
$C_{18}H_{37}OH$ [c]	Fe^{powder}| hexadecane	[d] | 18.55|	[d] 19| × a_p	0.0145	−10.99	0.34

[a] QCM data, 23 °C.
[b] From detention time in adsorption column [13], 22 °C.
[c] Depletion isotherms [10,11], Fe_2O_3 -terminated iron powder|hexadecane, 23 °C or 30 °C.
[d] |…| indicates fixed value; |… indicates value at the lower limit allowed by the optimization procedure; …| means upper limit.
[e] Deviation, Eq. (6).

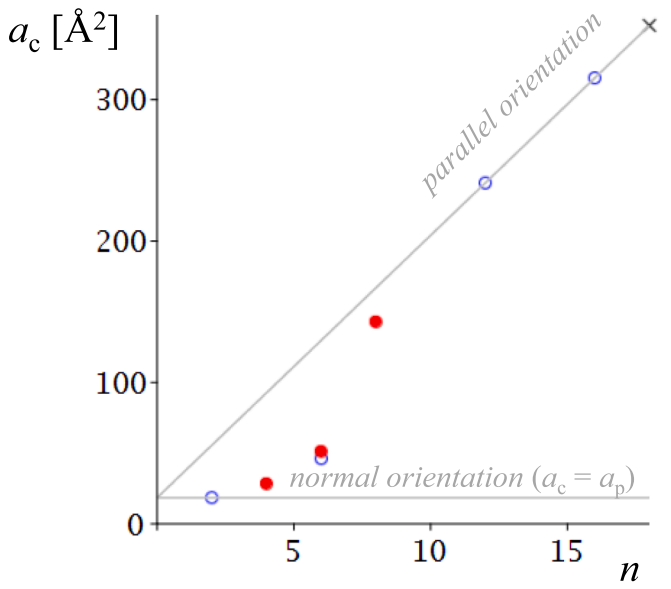

Fig. 4. Dependence of the area a_c per chemisorbed molecule on the chain length n of normal alcohols adsorbing at the Fe_2O_3|alkane interface. Empty circles are based on our QCM data; solid circles are based on data from ref. [13]; cross is based on ref. [10,11], see Table 1. The horizontal solid line corresponds to projected area of hydrocarbon chain normal to the surface ($\theta = 90°$); the inclined solid line stands for chain parallel to the surface ($\theta = 0°$).

The dependence of a_c on n in Fig. 4 indicates that short chained alcohols (ethanol, butanol) remain inclined at a high angle to the plane of the surface ($\theta > 70°$) upon chemisorption; in contrast, all higher alcohols (octanol-octadecanol) are approximately parallel to the surface ($\theta < 20°$). A transition between the two configurations appears at about $n = 6$, and hexanol shows an intermediate behaviour. Allen and Patel [13] discovered a related transition taking place at $n = 6$ in the adsorption heat of series of alkanols at Fe_2O_3|alkane.

3.7.2. Solvent effect

The adsorption isotherms of hexanol onto $Fe_2O_3^{QC}$ from three different hydrocarbon solvents – dodecane, isooctane and *tert*-butylbenzene – are shown in Fig. 5. Evidently, the nature of the solvent has a marked influence on the adsorption behaviour for the studied system, far more significant than what is observed, e.g., for alcohols at water|oil interfaces [81]. Both the initial slope and the plateau value of the isotherm are affected.

The CPL model (5) was used to interpret the data in Fig. 5. The area a_p per physisorbed molecule (or per site) was set equal to 18.5 Å^2, as found in the previous section. The other three parameters – a_c, x_c, and K_a – were found to change with the solvent (Table 2).

The physisorption constant K_a is significantly higher in isooctane (83 μm) and *tert*–butylbenzene (59 μm) than in dodecane (14 μm). This is probably due to a combination of effects: **(i)** the adsorption of hexanol requires the desorption of a solvent molecule, therefore, the difference in K_a might reflect high adsorption energy of the straight-chain dodecane compared to the branched hydrocarbons. Indeed, *n*-alkanes are known to adsorb on metal oxide surfaces with significant adsorption heats [82] and isooctane's branched structure makes the contact difficult. **(ii)** The difference between isooctane and *tert*–butylbenzene may be due to a similar reason (higher affinity of the benzene ring to the

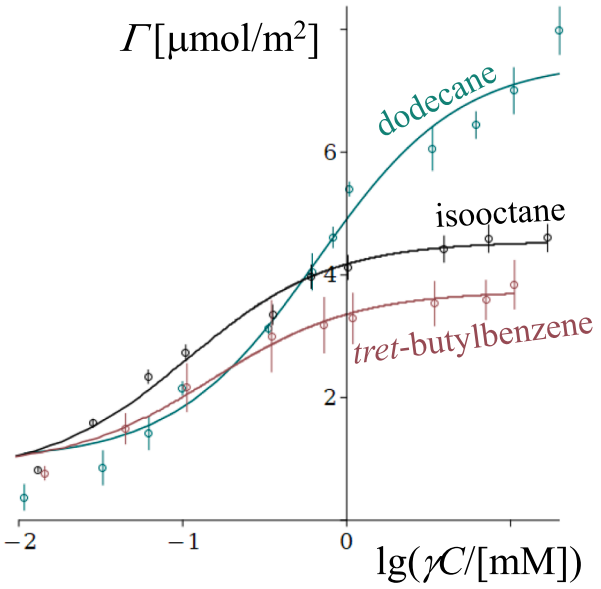

Fig. 5. Adsorption isotherms of hexanol from dodecane, isooctane and *tert*-butylbenzene on $Fe_2O_3^{QC}$ at room temperature. Lines: the CPL model (5), with the parameters from Table 2.

surface [36,83,84]) or due to *tert*-butylbenzene, as an aromatic hydrocarbon, being a better solvent [85] for the polar hexanol. **(iii)** The state of the physisorption sites may be affected by the solvent: the partial hydroxylation and water physisorption of the surface, the chemistry of the pre-adsorbed organic molecules etc. are likely to vary from solvent to solvent.

The orientation of the chemisorbed hexanol changes from intermediate in dodecane ($a_c = 2.49 \times a_p$) to parallel to the surface in isooctane and *tert*-butylbenzene ($a_c \approx 7 \times a_p$, see Table 2). Fig. 4 shows that hexanol is at a point of a fine balance, intermediate between the short alcohols standing normal and the long alcohols lying parallel to the surface. As a result, chemisorbed hexanol's orientation should vary more than that of any other alcohol. A branched hydrocarbon is a worse solvent for the straight-chain hexyl than *n*-dodecane, and *n*-dodecane should adsorb more strongly at the Fe_2O_3 surface. Therefore, isooctane favours parallel orientation of chemisorbed hexanol molecules more than dodecane.

The fraction of chemisorption sites x_c may be affected by the solvent indirectly, by the impurities present. The XPS data in Fig. S2 show chemisorbed organic impurities even on the pristine surface. Trace amounts of peroxides in the solvent (the primary product of autoxidation of hydrocarbons [59]) are likely to add up to this pre-chemisorbed material, i.e. the chemisorption sites can be partly occupied before the alcohol is introduced to the QCM cell. The fitted values show more chemisorption sites available in isooctane ($x_c = 16$ %) in comparison with dodecane ($x_c = 13$ %), and significantly increased x_c in *tert*-butylbenzene (23 %). One possible explanation is that, since *tert*-butylbenzene is resistant to autoxidation [59], less oxygen-containing impurities are pre-adsorbed and more chemisorption sites are free for the alcohol to occupy in this solvent.

The simultaneous change in K_a, a_c and x_c from one solvent to another leads to an interesting effect: at high concentration, the adsorption of hexanol is largest at Fe_2O_3|dodecane due to smaller area per chemisorbed molecule; at low concentrations, however, the hexanol adsorbs the least at Fe_2O_3|dodecane, due to small K_a and x_c (Fig. 5).

To confirm these observations, we investigated the adsorption of hexanol at steel^{QC}|dodecane and steel^{QC}|isooctane. Indeed, the adsorption data at these interfaces agree with $a_c = 2.49 \times a_p$ at steel^{QC}|dodecane and with $a_c \approx 7 \times a_p$ at steel^{QC}|isooctane, same as those for $Fe_2O_3^{QC}$ (see Table 2).

Similar trends were reported in the literature for other polar molecules. The adsorbed amounts of 4-n-nonylphenol on Fe_2O_3 was found to be higher in a mixture of dodecane (45 %) and isooctane (55 %) than in dodecane alone [14]. Bewig and Zisman [32] investigated the adsorption of primary amines on platinum from several alkanes: they found that adsorption from branched alkanes and aromatic solvents is lower than that from straight-chain alkanes, which agrees with our results in Fig. 5 at high *C*; also, adsorption from long chained hydrocarbons was found to be higher than that from short chained ones. Groszek [12] found that the adsorption of hexanol and octadecanol onto Fe_2O_3 and iron metal is higher in hexadecane than in heptane. These observations have been attributed to the formation of a mixed orientated film which includes solvent molecules. Allen and Patel [86] found butan-1-ol to adsorb on TiO_2 powder more strongly from heptane than from benzene and xylene, which they attributed to competitive adsorption between the hydrocarbon and the alcohol. Since their data are for monolayers close to saturation, we think instead that this may be an effect on the orientation similar to the one discussed above with hexanol (i.e. it comes from a_c, not K_a).

The solvent-specific trace level of water may be a factor in the observed trends, since removing water completely from the hydrocarbon is a challenge. Water hydroxylates the Fe_2O_3 surface; moreover, it can physisorb, and can associate with dissolved alcohol in the organic solvent. For example, the adsorption of octadecanol and octanol from dry xylene and heptane onto TiO_2 was higher than that from solutions containing traces of water [87,88], attributed to competition with water. The solubility of water in aliphatic hydrocarbons decreases slightly as the chain length increases [89,90] and it is higher in aromatic hydrocarbons than that in aliphatic ones. The degree of branching of the side chains decreases water solubility in aromatic hydrocarbons, but has the opposite effect in aliphatic hydrocarbons [89]. For our solvents, the water solubility at 20 °C decreases in the following order [89]: *tert*-butyl benzene (19.5 mM) > isooctane (7.9 mM) > dodecane (estimated 3.4 mM) > hexadecane (3.0 mM). The presence of more water in *tert*-butylbenzene could contribute to the observed decrease in absorption of hexanol compared to dodecane at high concentration. However, water explains neither the difference between dodecane and isooctane nor the adsorption behaviour at low concentration of hexanol.

3.7.3. Effect of the nature of the surface

From the discussion so far, it is already evident that the nature of the Fe_2O_3 surface changes depending on the way of preparation and the

Table 2
Role of the solvent and the surface on the adsorption parameters.

alcohol	interface	a_p [Å^2]	a_c	x_c	lnK_a[m]	δ_Γ[μmol/m^2]
$C_6H_{13}OH$	$Fe_2O_3^{QC}$|dodecane	18.55	$2.49 \times a_p$	0.1315	−11.20	see Table 1
$C_6H_{13}OH$	$Fe_2O_3^{QC}$|isooctane	|18.55|	$7\|\times a_p$	0.1616	−9.40	0.20
$C_6H_{13}OH$	$Fe_2O_3^{QC}$|*tert*-butylbenzene	|18.55|	$7\|\times a_p$	0.233	−9.74	0.18
$C_6H_{13}OH$	steel^{QC}|dodecane	|18.55|	$\|2.49\|\times a_p$	0.0855	−8.55	0.49
$C_6H_{13}OH$	steel^{QC}|isooctane	|18.55|	$\|7\|\times a_p$	0.053	−8.12	0.28
$C_6H_{13}OH$	$Fe_2O_3^{powder}$|isooctane	|18.55|	$\|7\|\times a_p$	0.050	−13.51	0.75
C_2H_5OH [14]	$Fe_2O_3^{powder}$|isooctane	|18.55|	$\|1\|\times a_p$	|0.050|	−13.10	0.6

|…| indicates fixed value, |… indicates value at the lower limit allowed by the optimization procedure; …| means at the upper limit.

actual material. This is informed by **(i)** the XP spectra (Fig. 1), and **(ii)** the difference between the parameters K_a and x_c of the adsorption isotherms for our $Fe_2O_3^{QC}$ and steel^{QC}, the iron powder of Nakayama and Studt, and the haematite powder of Allen and Patel (Table 1 and Table 2). To analyse the role of the surface, we compare in Fig. 6 the adsorption of hexanol at three different Fe_2O_3|isooctane surfaces, with Fe_2O_3 being the top layer of either haematite- or stainless steel-coated quartz crystal (QCM measurement), or of Fe_2O_3 powder (measured via the depletion method). Although all these surfaces are haematite-terminated, the preparation of the surface results in large differences in the measured adsorption.

The respective adsorption parameters of CPL are listed in Table 2. The physisorption area a_p was fixed to the value 18.5 Å^2 found before. We also fixed $a_c = 7 \times a_p$ (chemisorbed molecules parallel to the surface), as found in the previous section for hexanol at Fe_2O_3|isooctane. The values of x_c and K_a depend on the surface. Steel^{QC} has lower fraction of chemisorption sites than $Fe_2O_3^{QC}$ ($x_c = 5$ % compared to 16 %); the Fe_2O_3 powder is also of low x_c (5 %, like steel^{QC}). K_a is strikingly different for the three surfaces: very high for steel^{QC} (300 µm), and very low for Fe_2O_3 powder (1.4 µm), compared to 83 µm for $Fe_2O_3^{QC}$. We compared our results with data for hexanol at $Fe_2O_3^{powder}$|heptane of Allen and Patel [13]. Their Fe_2O_3 was found to have a similar adsorption constant to our powder, $K_a = 2$ µm, but with a higher fraction of chemisorption sites, $x_c = 22.5$ % (Table 1).

These trends were confirmed with a couple of additional measurements (see Table 2):

(i) We studied the adsorption of hexanol at steel^{QC}|dodecane (rather than isooctane). Fixed values of the areas $a_p = 18.5$ Å^2 and $a_c = 2.5 \times a_p$, as for $Fe_2O_3^{QC}$|dodecane, agree well with the data, i.e. the orientation of both physi- and chemisorbed molecules indeed seems to depend on the solvent but not on the nature of the surface. The number of chemisorption sites was again found to be smaller for steel^{QC} ($x_c = 8.5$ %) than for $Fe_2O_3^{QC}$|dodecane (13 %). The physisorption constant for steel^{QC}|dodecane is again very high ($K_a = 200$ µm).

(ii) We studied the adsorption of ethanol (rather than hexanol) at $Fe_2O_3^{powder}$|isooctane, using the depletion method. We investigated the data for below 6 mM only. We fixed the values of all parameters known from the previous sections: for ethanol, $a_p = a_c = 18.5$ Å^2, see Table 1; for $Fe_2O_3^{powder}$|isooctane, $x_c = 5$ % (obtained from the fit of the data for hexanol in Fig. 6). The only parameter left, the physisorption constant of ethanol, was obtained by regression as $K_a = 2$ µm, close to the value for hexanol. Above 6 mM, the measured apparent adsorption corresponds to multilayer coverage. While not impossible, it is unlikely that multilayer structure can form on Fe_2O_3 powder but not on Fe_2O_3-coated quartz crystal (see Fig. 3). The apparent multilayer adsorption may be an artifact due to capillary condensation in the pores of the powder or because of the alcohol inducing dispersion of the Fe_2O_3 particles (i.e. the specific surface of the powder may be increasing in the presence of excess of alcohol).

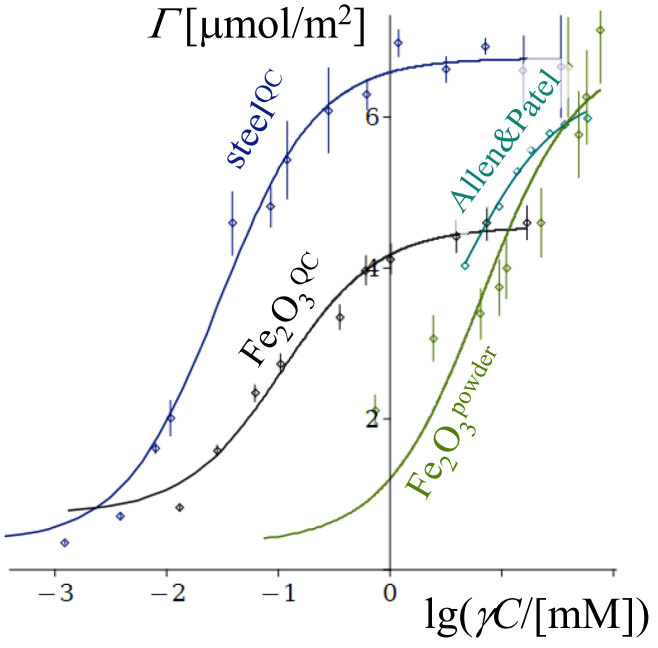

Fig. 6. Adsorption isotherms of hexanol from isooctane onto Fe_2O_3 for different haematite surfaces. Solid lines are Eq. (5) with the parameters from Table 2. The data by Allen and Patel [13] for hexanol at $Fe_2O_3^{powder}$|heptane are given for comparison.

3.7.4. *Effect of the position of the functional group and chain branching*

Position of the functional group. Fuel additives often have a branched hydrocarbon chain, and their functional groups are often attached at a secondary or tertiary carbon. Moreover, autoxidation typically produces secondary and tertiary alcohols. Therefore, we investigated the role of the position of the functional group on the adsorption of hexan-*m*-ol at $Fe_2O_3^{QC}$|dodecane, where $m = 1, 2, 3$. The measured adsorption decreases in the series $\Gamma_{\text{hexan-1-ol}} > \Gamma_{\text{hexan-2-ol}} > \Gamma_{\text{hexan-3-ol}}$ (Fig. 7); both the initial slope and the plateau value of the isotherm are affected in the same direction.

The data were compared to CPL, with the fraction of chemisorption sites fixed to the value $x_c = 13$ % found for $Fe_2O_3^{QC}$|dodecane above (Table 1). The fits are illustrated in Fig. 7; the CPL parameters are listed in Table 3. While independent of the length n of the chain of normal alcohols, the area a_p per physisorbed molecule increases with m ($a_{p,\text{hexan–1–ol}} < a_{p,\text{hexan-2-ol}} < a_{p,\text{hexan-3-ol}}$). This is expected – when the functional group that binds the surface is in the middle of the alkyl chain, it drags the adjacent CH_2 moieties onto the surface. The value for hexan–3–ol, 34 Å^2, is close to that of two sites overlaid by the two chain fragments, C_2H_5– and –C_3H_7, in C_2H_5–CHOH–C_3H_7. The value of a_p for physisorbed hexan-2-ol is intermediate between those for hexan-1-ol and hexan-3-ol. The fitted value for a_c suggests that, unlike hexan-1-ol, the chemisorbed hexan-2-ol lies flat on the surface (covering ≈7 sites). However, for chemisorbed hexan–3–ol, it appears that the –CHOH–C_3H_7 fragment is parallel to the surface but C_2H_5–is normal to it, not covering additional sites, resulting in ≈5 sites covered. Finally, the physisorption constants K_a of hexan–1–ol (14 µm) and hexan-2-ol

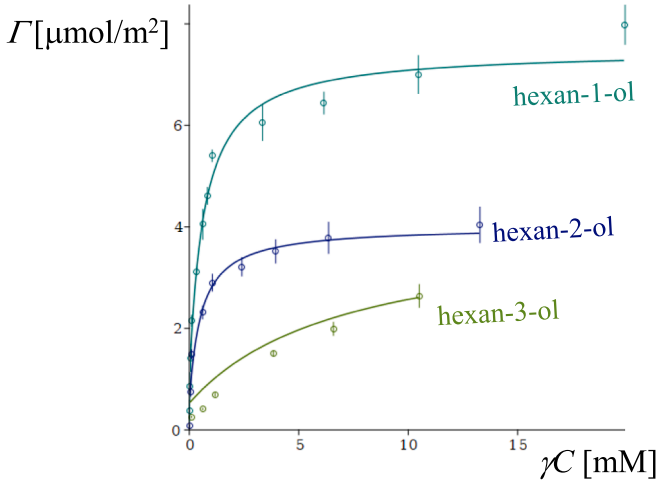

Fig. 7. Effect of the position of the functional group on the adsorption of hexan-*m*-ol for $m = 1,2,3$ at $Fe_2O_3^{QC}$|dodecane.

Table 3
The parameters of the CPL model for alcohols at the alkane|haematite interface.

alcohol	interface	a_p [Å^2]	a_c [Å^2]	x_c	ln(K_a/[m])	δ_Γ [μmol/m^2]
hexan-1-ol [a]	$Fe_2O_3^{QC}$|n-$C_{12}H_{26}$	18.55	2.49 × 18.55	0.1315	−11.20	see Table 1
hexan-2-ol [a]	$Fe_2O_3^{QC}$|n-$C_{12}H_{26}$	28.1	6.96 × 18.55	|0.1315|	−11.41	0.31
hexan-3-ol [a]	$Fe_2O_3^{QC}$|n-$C_{12}H_{26}$	34.2	4.75 × 18.55	|0.1315|	−14.20	0.32
$C_{18}H_{37}OH$ [b]	Fe^{powder}|n-$C_{16}H_{34}$	[c] |18.55|	[c] 19|×18.55	0.0145	−10.99	0.34
cyclohexanol [b]	Fe^{powder}|n-$C_{16}H_{34}$	42.1	2 × 42.1	|0.0145|	−12.29	0.13
2-ethylhexan-1-ol [a]	$Fe_2O_3^{QC}$|isooctane	32.03	6.97 × 18.55	|0.1616|	−11.57	0.18

[a] Our QCM data.
[b] Data from ref. [10,11], depletion method, 23 °C or 30 °C.
[c] |…| indicates fixed value, |… indicates value at the lower limit allowed by the optimization procedure; …| means at the upper limit.

(11 μm) are similar, but hexan-3-ol physisorbs less strongly (0.7 μm). One should keep in mind that, strictly speaking, the simple CPL model (5) is inapplicable for a system where the area per molecule (30–40 Å^2 for hexan-2-ol and hexan-3-ol) is significantly larger than the area per site (≈15-18 Å^2) – when this is the case, instead of Langmuir's isotherm, Everett's model must be used for $\Gamma_{physisorption}$ (where one physisorbed molecule covers multiple sites [91]). Such an analysis is complicated and is more appropriate for a dedicated future work, but we expect that the fitted value of K_a will be strongly affected.

Cyclohexanol. We supplemented our measurements with analysis of the data by Nakayama and Studt [10] for cyclohexanol at the iron^{powder}| hexadecane interface (see Fig. S7 in S4). We assumed that the fraction of chemisorption sites is unchanged in comparison with x_c = 1.5 % obtained for octadecanol on the same powder (see Table 1). Since x_c is so low on this interface, the chemisorbed cyclohexanol is of small amount and, as a result, the area of the chemisorbed alcohol is not a very sensitive parameter. We therefore chose for it the value $a_c = 2 \times a_p$ (alternative choices in the range $a_c = 1 \times a_p$ …$3 \times a_p$ lead to similar results). Two free parameters remain: the fit of the data with Eq. (5) yields a_p = 42 Å^2 (reasonable for cyclohexanol standing upright) and K_a = 4.6 μm (compared to 17 μm for octadecanol). Thus, the CPL analysis indeed yields realistic areas, and the tendency that the adsorption constant is lower for secondary alcohols than for primary is confirmed.

Chain branching. To study the role of branching, we measured the adsorption of 2–ethylhexan-1-ol at $Fe_2O_3^{QC}$|isooctane. It follows the CPL isotherm, with a_p = 32 Å^2 (intermediate between a_p of hexan-2-ol and hexan-3-ol), $a_c = 7 \times a_p$ (around 7 sites covered by the chemisorption molecule, as for hexan-1-ol in isooctane) and K_a = 9 μm (compared to 83 μm for hexan-1-ol at the same interface). The value of the fraction of chemisorption sites was fixed to x_c = 16 %, as obtained previously (see Table 2). Thus, the effect of branching is similar to the effect of changing the position of the functional group: a_p increases, K_a decreases.

However, several other experiments showed unusually high adsorption of branched alcohols, significantly higher than that of hexan-1-ol. This was the case at $Fe_2O_3^{QC}$|dodecane with both 2–ethylhexan-1-ol and 2-methylpentan-2-ol (Fig. S8). The high adsorption can be either due to multilayer formation, oxidation of the adsorbed branched alcohol or fragmentation of the molecule at the surface. However, it is unclear why this phenomenon takes place in dodecane but not in isooctane. We also studied the adsorption of 2–ethylhexan-1-ol at steel^{QC}|isooctane; adsorption was again higher than the simple CPL model could explain.

3.7.5. Temperature

The effect of temperature on the adsorption of hexan-1-ol at $Fe_2O_3^{QC}$| dodecane was investigated. As shown in Fig. 8, the adsorption decreases as T increases, indicating an exothermic process. This is unsurprising for adsorption driven by hydrogen bonding [31,13,14,92,93] and for iron alkoxide formation. What is surprising is the strong effect of T on the plateau value of the adsorption: the higher the temperature, the larger the limiting area per molecule (less absorbed alcohol is sufficient to cover the surface completely).

We compared the data with our model (5), under the following

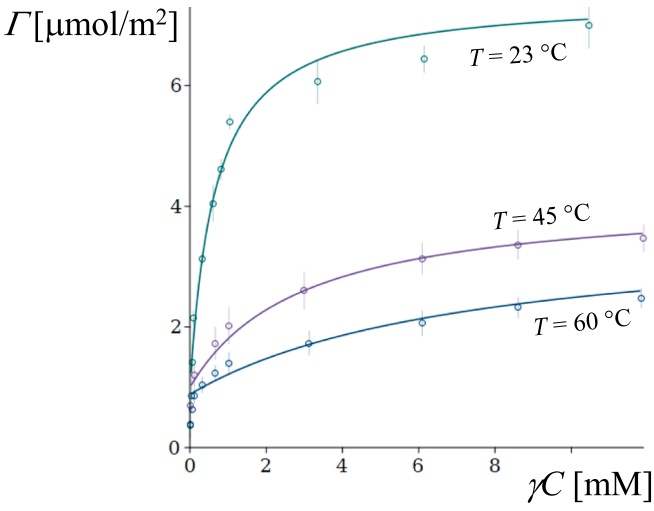

Fig. 8. Adsorption isotherms of hexanol from dodecane onto $Fe_2O_3^{QC}$ at several temperatures. Solid lines represent the fitting to the CPL model (5), with the parameters from Table S1.

assumptions: **(i)** the area per physisorbed molecule (or per site) remains constant, a_p = 18.5 Å^2. From our experience with adsorption at fluid interfaces at varying T, this is reasonable for the projected cross-sectional area of the hydrophobic chain [94,95]. **(ii)** The physisorption constant follows a Van 't Hoff dependence, ln $K_a(T)$ = ln K_a(296 K)–$\Delta_a H/R \times (1/T - 1/296\ K)$, where $\Delta_a H$ is the heat of physisorption and R is the gas constant. Since we know the parameters at 23 °C (see Table 1), we are left with 5 unknowns: a_c and x_c at 45 °C and 60 °C, and $\Delta_a H$. Fitting the data at 45 °C and 60 °C simultaneously leads to the parameters in Table S1 in S4. The area a_c per chemisorbed molecule increases with T – from 2.5 sites covered at 23 °C to 6–7 at 45–60 °C. A possible explanation is that at the higher temperature the solvent dodecane molecules desorb, which allows the hexyl chain of the chemisorbed $C_6H_{13}OH$ to attach to the surface. The fraction x_c of chemisorption sites increases from 13 % to 24 % at 45 °C, and it does not change further at 60 °C. This could be due to partial desorption of H_2O and adventitious organics from the chemisorption sites. Finally, the heat of physisorption is $\Delta_a H = -53.8$ kJ/mol; this corresponds to two O:–HO bonds per alcohol, or perhaps a coordination bond to an iron atom. The large enthalpy of adsorption results in a significant decrease in K_a with T (14, 3.0 & 1.2 μm for 23, 45 & 60 °C).

To support these findings, the data by Nakayama and Studt for octadecanol at iron^{powder}|hexadecane, studied at room temperature and at 65 °C, were reanalysed (unfortunately it is unclear from ref. [10,11] whether 'room temperature' refers to 23 °C or 30 °C). In this case, a_p = 18.5 Å^2 and $a_c = 19 \times a_p$ were fixed, leaving two fitting parameters at 65 °C, x_c and K_a. The data are presented in Fig. S9. The fit produced x_c = 3.8 %, i.e. the fraction of chemisorption sites increases with T again. The adsorption constant drops from K_a = 6.2 μm at room temperature to 4.7

μm at 65 °C. This corresponds to heat of adsorption of $\Delta_a H = -25.3$ or –31.1 kJ/mol (depending on whether "room temperature" means 23 °C or 30 °C). Thus, for the iron powder studied by Nakayama and Studt, the heat of physisorption is lower than for the Fe_2O_3-coated quartz crystal we studied, and corresponds to one O:–HO hydrogen bond. Similar trends appear to be followed also by other polar compounds onto different solid|hydrocarbon interfaces [31,13,14].

4. Conclusions

The main conclusion from this study is that, on haematite-terminated surfaces, alcohols adsorb as two distinct fractions: chemisorbed (chemically bound alcoholate FeO-O-R and products of its oxidation) and physisorbed (hydrogen-bonded, like FeO-OH—HOR, Fe_2O_3—HOR etc.). The XP spectra provide direct evidence for this. This is hardly surprising – it is well known that the same is true for water [39,40,73], and also for alcohol vapours [29,69]; however, few studies of adsorption of polar organics consider both fractions, especially from solvent, and even fewer provide a quantitative analysis of the combined adsorption [31].

A realistic adsorption isotherm model must take the chemisorption into account. Therefore, we developed a version of the Langmuir model with chemisorption (CPL, Eq. (5)), which treats explicitly the two populations of surface sites and adsorbed alcohol molecules. It builds up on work done for water [73] but tuned to organic molecules, and is an improvement over existing models of adsorption of fuel and lubricant additives, corrosion inhibitors etc. on metal oxides, which neglect either the chemisorption or the physisorption.

CPL has four parameters of clear physical meaning: the areas a_p and a_c per physisorbed and chemisorbed alcohol, the fraction x_c of chemisorption sites at the surface, and the physisorption constant K_a. We studied the dependence of these parameters on the nature of the system and the conditions, by measuring and analysing a large body of QCM data. We varied the alkanol structure, the solvent, the nature of the haematite surface, the temperature. We also analysed literature data for alkanols with CPL, to demonstrate that the model captures well the physical chemistry of this class of systems.

We found that the height of the plateau and the shape of the adsorption isotherm depend strongly on the orientation of the chemisorbed molecules. Long normal alkanols tend to assume parallel orientation upon chemisorption, hence covering large area a_c (Fig. 9). Thus, relatively few chemisorbed dodecanol and hexadecanol molecules are sufficient to cover 66–72 % of the available surface, leaving little space for physisorption and producing flattish isotherms. By contrast, short homologues and branched alcohols assume upright configuration upon chemisorption and the total adsorption is dominated by physisorption. When the solvent is a normal alkane, hexanol marks the boundary between these two limiting behaviours (Fig. 4). The transition in adsorption behaviour at $C_6H_{13}-$ has been detected empirically half a century ago [13], but we provide for the first time the explanation, allowed by the explicit account for chemisorption in CPL.

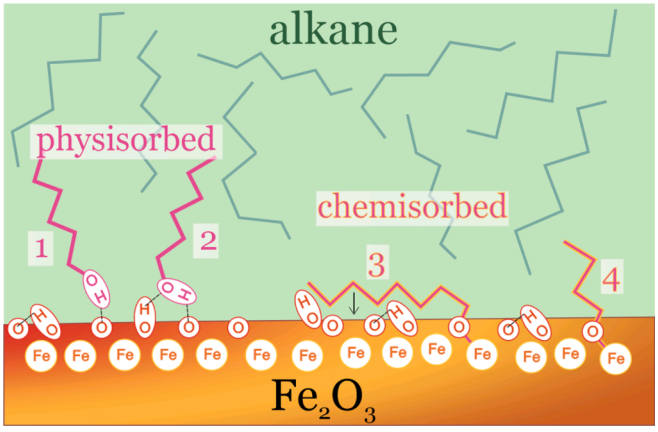

Fig. 9. Four populations of adsorbed alcohols on Fe_2O_3-terminated surfaces identified in this study: (1) physisorbed alkanol bound with a single hydrogen bond to the surface; (2) physisorbed, two hydrogen bonds; (3) chemisorbed long alcohol, parallel to the surface; (4) chemisorbed short alcohol, normal.

The presence of chemisorption in the adsorption model means that the adsorption isotherm is sensitive to the initial state of the surface, including level of hydroxylation, dominant crystal faces, surface defects, pre-adsorbed adventitious organics occupying a fraction of the chemisorption sites. This is demonstrated by Fig. 6 and the XPS data in S2. The CPL analysis of the QCM data demonstrates that the area parameters a_p and a_c are independent of the surface. However, the fraction x_c of chemisorption sites changes from 1.5 % for iron powder, past 5–9 % for steel^{QC} and 13–16 % for $Fe_2O_3^{QC}$, up to 23 % for Fe_2O_3 powder. The physisorption constant K_a varies even more dramatically – by two orders of magnitude (Table 2).

The temperature dependence of the adsorption is also well captured by CPL. The isotherm is affected by T not only through the trivial Van 't Hoff dependence of the physisorption constant K_a; the fraction of chemisorption sites also increases – for the surfaces we studied, it doubles at 45–60 °C compared to room temperature, resulting in a significant drop of the isotherm plateau (Fig. 8 and Table S1). The shift of the plateau with T is also a well-known phenomenon [10,11,31] that cannot be explained by a model considering physisorption only.

Limitations and future work. The CPL model is a simplified version of reality. Although it captures well much of the adsorption behaviour observed experimentally, it has four important limitations. One obvious difficulty is that the molar mass of chemisorbed and physisorbed alcohol can be different. For example, one possible chemisorption process is:

$$\text{FeO-OH} + C_nH_{2n+1}OH \rightarrow \text{FeO-O}C_nH_{2n+1} + H_2O.$$

For chemisorption of ethanol, this reaction corresponds to increase in mass of the solid by 28.1 g/mol (EtO- substitutes HO–), compared to 46.1 g/mol for physisorbed ethanol. If the water produced by the reaction remains on the surface, then the mass increase per ethanol chemisorption event will be 46.1 g/mol, as for physisorption, but then the newly adsorbed water provides a new adsorption site, which is not reflected by CPL. There are other possible chemisorption reactions, e.g., $Fe_2O_3 + 2ROH \rightarrow Fe_2O_2(OR)_2 + H_2O$, subsequent oxidation of the adsorbed alcohol etc. Since we could not identify the dominant chemisorption process, we assumed that the mass added to the QC per adsorption event is equal to the molar mass of the alcohol. This approximation affects mostly the data for the short chained alcohols.

The second limitation of CPL is that it assumes the population of physisorbed alcohol is uniform, having the same binding energy to the surface. The variability of the value of the physisorption constant K_a (from 1.4 μm for haematite powder|isooctane to 300 μm for steel^{QC}|isooctane, see Table 2) and the heat of physisorption (from 25 to 54 kJ/mol) is a clear proof that several kinds of physisorption sites coexist at haematite-terminated surfaces. The most probable source of variability is the surface density of hydroxyl. Surface –OH groups are classified into isolated OH and hydrogen bonded OH. The distribution of these groups depends on T, acidity, humidity and the preparation method [96,97]. Heating of α-Fe_2O_3 powder to only 373 K is sufficient to reduce significantly the number of H-bonded hydroxyl group via condensation of adjacent OH groups [43]. On neat Fe_2O_3, alcohols will form a single hydrogen bond with the surface (hydrogen from ROH to oxygen from Fe_2O_3, Fig. 9). Next to an isolated single hydroxyl group, two hydrogen bonds will be formed (the second will be hydrogen from FeO-OH to oxygen in ROH, Fig. 9), causing much stronger adsorption. At high density of hydroxyls, the oxygen available at the surface will be already saturated with hydrogen bond from adjacent hydroxyls, and the physisorption will be weakened again. On top of the variability in hydroxylation, the studied surfaces correspond to a mixture of crystal faces, and the physisorption on each face is of different strength. The surface of the coated QC plates were in prolonged contact with air; therefore, they should be oxygen- and –OH terminated (i.e. R-Fe-Fe-O_3, R-{Fe-Fe-O_2}-

$(OH)_2$, or partially reduced forms such as R–{O_3–Fe-Fe}-O-OH and R-{O_3-Fe-Fe}-$(OH)_3$ that are of zero dipole moment). However, the termination of the powders may be iron-terminated (R-Fe-O_3-Fe, or a hydroxylated variant of this [15,16]); in such case, the physisorption of alcohols may be through coordination bond rather than H-bond. Also, stainless steel contains Cr in the top Fe_2O_3 layer.

A third limitation of CPL is the assumption that the area per site (perhaps ~ 15 Å^2) is equal to the area per physisorbed molecule. This is not fulfilled even for normal alkanols (cross-sectional area 18.5 Å^2, i.e. each physisorbed alcohol covers 1.2 sites), and is a serious approximation for branched alkanols which could cover 2–3 sites per physisorbed molecule. Everett's isotherm [91] should be used instead of Langmuir's Eq. (4) to account for this effect.

Finally, we assumed that the chemisorption sites are completely covered at any nonzero concentration of the adsorbing alcohol [31]. This is rarely true: at low concentration, we often see adsorption lower than expected from the CPL model alone (the first few points of the isotherm of hexanol in Fig. 3a are an example; cf. also water chemisorption [15] reaching a plateau at relative humidity of 10^{-7}). This can be taken into account by substituting Eq. (3) for a Langmuir or Everett isotherm of a high chemisorption constant K_c (like McCafferty & Zettlemoyer's model for water [73]). We suspect, however, that the experimental effect may be kinetic rather than thermodynamic. The stepwise protocol we used for QCM measurement allows many hours for relaxation of the chemisorbed fraction for the concentrated alcohol solutions, but the least concentrated solutions have 30 min for equilibration, which may be insufficient (see S3).

Some of our results are artifacts due to these limitations. For example, the dependence of the physisorption constant on the chain length of the alkanol (Fig. S6 and Table 1) can be explained with the existence of a fraction of strong physisorption sites that is accessible to small molecules only. Another option is that chemisorption is localized in energy-rich regions of the surface (e.g., next to step defects), and in these regions physisorption is also stronger. If this is the case, the chemisorption of large molecules will block preferentially strong physisorption sites, effectively reducing K_a. Both scenarios cannot be analysed based on Eq. (5) alone.

Let us finally briefly compare the Fe_2O_3|hydrocarbon interface with Fe_2O_3|water and Fe_2O_3|air. Fe_2O_3|air is similar to Fe_2O_3|hydrocarbon in terms of (i) variability; (ii) significant chemisorption [73,29,69]; (iii) alcohol physisorption is driven mostly by hydrogen bonding on both interfaces. However, on Fe_2O_3|air, the alkyl-Fe_2O_3 Van der Waals interaction contributes to the adsorption, resulting in higher adsorption of higher alcohols at a fixed vapour pressure [29,69]. In contrast, on Fe_2O_3|hydrocarbon, the desorption of alkane solvent cancels the Van der Waals contribution to alkanol adsorption [98]. In addition, the significant lateral alkyl-alkyl Van der Waals attraction renders Langmuir's isotherm unsuitable for Fe_2O_3|air – attraction has to be accounted for (e.g., through Frumkin's isotherm).

Fe_2O_3|water, however, is a very different interface. First, water binds all chemisorption sites, and the haematite surface will be completely hydrated, and therefore not as variable. Water competes for the hydrogen bonds at the surface with the alcohol; moreover, similarly to the hydrocarbon solvents, it cancels the Van der Waals component in the adsorption energy (water has Hamaker constant similar to that of alkanes [98]). The existing data [99] suggest that the adsorption of alcohols on Fe_2O_3|water is driven by the hydrophobic effect – as indicated by the fact that Traube's rule is approximately followed. Finally, as with Fe_2O_3|air (but unlike Fe_2O_3|oil), lateral cohesion is a feature of alkanol monolayers on Fe_2O_3|water [99].

CRediT authorship contribution statement

Ibrahim E. Salama: Writing – original draft, Visualization, Methodology, Investigation, Formal analysis, Data curation. **Radomir I. Slavchov:** Writing – review & editing, Writing – original draft, Software, Methodology, Investigation, Funding acquisition, Formal analysis, Conceptualization. **Sorin V. Filip:** Resources, Project administration, Funding acquisition, Conceptualization. **Stuart M. Clarke:** Writing – review & editing, Supervision, Resources, Project administration, Methodology, Conceptualization.

Declaration of competing interest

The authors declare that they have no known competing financial interests or personal relationships that could have appeared to influence the work reported in this paper.

Acknowledgements

The funding and technical support from bp through the bp International Centre for Advanced Materials (bp-ICAM) made this research possible. The expertise of Dr Shaoliang Guan, who performed the XPS measurements, is gratefully acknowledged.

Appendix A. Supplementary data

Supplementary data to this article can be found online at https://doi.org/10.1016/j.jcis.2025.01.086.

Data availability

Data will be made available on request.

References

[1] A. Elfasakhany, Performance and emissions of spark-ignition engine using ethanol–methanol–gasoline, n-butanol–iso-butanol–gasoline and iso-butanol–ethanol–gasoline blends: a comparative study, Eng. Sci. Technol. 19 (4) (2016) 2053–2059, https://doi.org/10.1016/j.jestch.2016.09.009.
[2] M. Mourad, K.R.M. Mahmoud, Performance investigation of passenger vehicle fueled by propanol/gasoline blend according to a city driving cycle, Energy 149 (2018) 741–749, https://doi.org/10.1016/j.energy.2018.02.099.
[3] M. Mourad, K. Mahmoud, Investigation into SI engine performance characteristics and emissions fuelled with ethanol/butanol-gasoline blends, Renew. Energy 143 (2019) 762–771, https://doi.org/10.1016/j.renene.2019.05.064.
[4] A.K. Thakur, A.K. Kaviti, R. Mehra, K.K.S. Mer, Progress in performance analysis of ethanol-gasoline blends on SI engine, Renew. Sustain. Energy Rev. 69 (2017) 324–340, https://doi.org/10.1016/j.rser.2016.11.056.
[5] J. Campos-Fernández, J.M. Arnal, J. Gómez, M.P. Dorado, A comparison of performance of higher alcohols/diesel fuel blends in a diesel engine, Appl. Energy 95 (2012) 267–275, https://doi.org/10.1016/j.apenergy.2012.02.051.
[6] L. Yao, F. Qi, X. Tan, X. Lu, Improved production of fatty alcohols in cyanobacteria by metabolic engineering, Biotechnol. Biofuels 7 (1) (2014) 94, https://doi.org/10.1186/1754-6834-7-94.
[7] J.G. Speight, in: The chemistry and technology of petroleum, fifth ed., CRC Press, 2014 https://doi.org/10.1201/b16559.
[8] V.M. Kapustin, Petroleum and alternative fuels with additives and dopants, KolosS, Moscow, 2008, p. 116.
[9] R.I. Slavchov, M. Salamanca, D. Russo, I. Salama, S. Mosbach, S.M. Clarke, M. Kraft, A.A. Lapkin, S.V. Filip, The role of NO_2 and NO in the mechanism of hydrocarbon degradation leading to carbonaceous deposits in engines, Fuel 267 (2020) 117218, https://doi.org/10.1016/j.fuel.2020.117218.
[10] K. Nakayama, P. Studt, The adsorption of polar cyclic compounds on iron surfaces from hydrocarbon solutions and their lubricating properties, Wear 116 (1) (1987) 107–118, https://doi.org/10.1016/0043-1648(87)90271-7.
[11] K. Nakayama, P. Studt, Additive interaction and lubrication performance in a polar additive binary system, Tribol. Int. 24 (3) (1991) 185–191, https://doi.org/10.1016/0301-679X(91)90025-5.
[12] A.J. Groszek, Heats of preferential adsorption of boundary additives at iron oxide/liquid hydrocarbon interfaces, ASLE Trans. 13 (4) (1970) 278–287, https://doi.org/10.1080/05698197008972303.
[13] T. Allen, R.M. Patel, Adsorption of alcohols on finely divided powders, J. Appl. Chem. 20 (6) (1970) 165–171, https://doi.org/10.1002/jctb.5010200601.
[14] R.M. Alloway, J. Mong, I.W. Jephson, M.H. Wood, M.T.L. Casford, P. Grice, S. V. Filip, I.E. Salama, C. Durkan, S.M. Clarke, Adsorption of 4-*n*-nonylphenol, carvacrol, and ethanol onto iron oxide from nonaqueous hydrocarbon solvents, Langmuir 35 (36) (2019) 11662–11669, https://doi.org/10.1021/acs.langmuir.9b01863.
[15] S. Yamamoto, T. Kendelewicz, J.T. Newberg, G. Ketteler, D.E. Starr, E.R. Mysak, K. J. Andersson, H. Ogasawara, H. Bluhm, M. Salmeron, G.E. Brown, A. Nilsson, Water Adsorption on α-Fe $_2$ O $_3$ (0001) at near Ambient Conditions, J. Phys. Chem. C 114 (5) (2010) 2256–2266, https://doi.org/10.1021/jp909876t.

[16] E. Voloshina, Hematite, Its Stable Surface Terminations and Their Reactivity Toward Water, in: Encyclopedia of Interfacial Chemistry, Elsevier, 2018, pp. 115–121, https://doi.org/10.1016/B978-0-12-409547-2.14157-5.

[17] F. Kraushofer, Z. Jakub, M. Bichler, J. Hulva, P. Drmota, M. Weinold, M. Schmid, M. Setvin, U. Diebold, P. Blaha, G.S. Parkinson, Atomic-Scale Structure of the Hematite α-Fe_2O_3 (1$\bar{1}$02) "R-Cut" Surface, J. Phys. Chem. C 122 (3) (2018) 1657–1669, https://doi.org/10.1021/acs.jpcc.7b10515.

[18] X.-G. Wang, W. Weiss, Sh. Shaikhutdinov, M. Ritter, M. Petersen, F. Wagner, R. Schlögl, M. Scheffler, The Hematite (α- Fe2O3) (0001) Surface: Evidence for Domains of Distinct Chemistry, Phys. Rev. Lett. 81 (5) (1998) 1038–1041, https://doi.org/10.1103/PhysRevLett.81.1038.

[19] L. Schöttner, R. Ovcharenko, A. Nefedov, E. Voloshina, Y. Wang, J. Sauer, C. Wöll, Interaction of Water Molecules with the α-Fe_2O_3 (0001) Surface: A Combined Experimental and Computational Study, J. Phys. Chem. C 123 (13) (2019) 8324–8335, https://doi.org/10.1021/acs.jpcc.8b08819.

[20] P. Liu, T. Kendelewicz, G.E. Brown, E.J. Nelson, S.A. Chambers, Reaction of water vapor with α-Al_2O_3(0001) and α-Fe_2O_3(0001) surfaces: synchrotron X-ray photoemission studies and thermodynamic calculations, Surf. Sci. 417 (1) (1998) 53–65, https://doi.org/10.1016/S0039-6028(98)00661-X.

[21] G. Busca, V. Lorenzelli, Infrared study of CO_2 adsorption on haematite, Mater. Chem. 5 (3) (1980) 213–223, https://doi.org/10.1016/0390-6035(80)90044-9.

[22] N.S. Clarke, P.G. Hall, Adsorption of water vapor by iron oxides. 1. Preparation and characterization of the adsorbents, Langmuir 7 (4) (1991) 672–677, https://doi.org/10.1021/la00052a014.

[23] J. Poon, D.C. Madden, M.H. Wood, S.M. Clarke, Characterizing Surfaces of Garnet and Steel, and Adsorption of Organic Additives, Langmuir 34 (26) (2018) 7726–7737, https://doi.org/10.1021/acs.langmuir.8b01405.

[24] A. Krautsieder, N. Sharifi, D.C. Madden, J. Sonke, A.F. Routh, S.M. Clarke, Corrosion inhibitor distribution on abrasive-blasted steels, J. Colloid Interface Sci. 634 (2023) 336–345, https://doi.org/10.1016/j.jcis.2022.12.003.

[25] S. Lee, R.W. Staehle, Adsorption of Water on Copper, Nickel, and Iron, Corrosion 53 (1) (1997) 33–42, https://doi.org/10.5006/1.3280431.

[26] J.J. Hamon, A. Striolo, B.P. Grady, Observing the effects of temperature and surface roughness on cetyltrimethylammonium bromide adsorption using a quartz-crystal microbalance with dissipation monitoring, J. Surfact. Deterg. 22 (2019) 1201, https://doi.org/10.1002/jsde.12294.

[27] L.J. Farren, N. Sharifi, S.M. Clarke, R.I. Slavchov, Effect of the solvent quadrupolarizability on the strength of the hydrogen bond: theory vs data for the Gibbs energy and enthalpy of homo- and heteroassociation between carboxylic acids and water, J. Chem. Phys. 158 (21) (2023) 214503, https://doi.org/10.1063/5.0137052.

[28] G. Beamson, D. Briggs, High resolution XPS of organic polymers: the Scienta ESCA300 database, John Wiley, Chichester, UK, 1992.

[29] G. Busca, Infrared study of methanol, formaldehyde, and formic acid adsorbed on hematite, J. Catal. 66 (1) (1980) 155–161, https://doi.org/10.1016/0021-9517(80)90017-2.

[30] R.I. Slavchov, S. Mosbach, M. Kraft, R. Pearson, S.V. Filip, An adsorption-precipitation model for the formation of injector external deposits in internal combustion engines, Appl. Energy 228 (2018) 1423–1438, https://doi.org/10.1016/j.apenergy.2018.06.130.

[31] J.J. Kipling, in: Adsorption from Solutions of Non-Electrolytes, Elsevier, 1965, p. 102, https://doi.org/10.1016/C2013-0-12353-7.

[32] K.W. Bewig, W.A. Zisman, Investigation of solution adsorption on platinum of pure and mixed films of fatty amines by contact potentials, J. Phys. Chem. 67 (1) (1963) 130–135, https://doi.org/10.1021/j100795a031.

[33] R. Aveyard, B.J. Briscoe, J. Chapman, Activity coefficients and association of n-alkanols in n-octane, J. Chem. Soc., Faraday Trans. 1 69 (1973) 1772, https://doi.org/10.1039/f19736901772.

[34] D. Brune, G. Hultquist, Corrosion of a stainless steel with low nickel content under static conditions, Biomaterials 6 (1985) 265–268, https://doi.org/10.1016/0142-9612(85)90023-7.

[35] H. Uddenberg, Q-Sense E4 operator manual: including the acquisition software QSoft 401, Q-Sense AB, Sweden, 2009.

[36] G. Sauerbrey, Verwendung von Schwingquarzen zur Wägung dünner Schichten und zur Mikrowägung, Zeitschrift Für Physik 155 (2) (1959) 206–222, https://doi.org/10.1007/BF01337937.

[37] M. Rodahl, F. Höök, A. Krozer, P. Brzezinski, B. Kasemo, Quartz crystal microbalance setup for frequency and Q -factor measurements in gaseous and liquid environments, Rev. Sci. Instrum. 66 (1995) 3924–3930, https://doi.org/10.1063/1.1145396.

[38] Knock, M. M., Sanii, L. S. (2011). Effect of hydrophobization of gold QCM-D crystals on surfactant adsorption at the solid-liquid interface. In *Amphiphiles: Molecular Assembly and Applications*; Nagarajan, R., Ed.; American Chemical Society: Washington, DC; Vols. 1070, pp. 175–192. DOI: 10.1021/bk-2011-1070.ch011.

[39] N.S. Clarke, P.G. Hall, Adsorption of water vapor by iron oxides. 2. Water isotherms and x-ray photoelectron spectroscopy, Langmuir 7 (4) (1991) 678–682, https://doi.org/10.1021/la00052a015.

[40] G. Blyholder, E.A. Richardson, Infrared and volumetric data on the adsorption of ammonia, water, and other gases on activated iron(III) oxide, J. Phys. Chem. 66 (12) (1962) 2597–2602, https://doi.org/10.1021/j100818a062.

[41] C. Ostwald, H.J. Grabke, Initial oxidation and chromium diffusion. I. Effects of surface working on 9–20% Cr steels, Corros. Sci. 46 (5) (2004) 1113–1127, https://doi.org/10.1016/j.corsci.2003.09.004.

[42] I. Iordanova, K.S. Forcey, R. Harizanova, Y. Georgiev, M. Surtchev, Investigation of structure and composition of surface oxides in a high chromium martensitic steel, J. Nucl. Mater. 257 (2) (1998) 126–133, https://doi.org/10.1016/S0022-3115(98)00446-2.

[43] L. Ferretto, A. Glisenti, Study of the surface acidity of an hematite powder, J. Mol. Catal. A Chem. 187 (2002) 119–128, https://doi.org/10.1016/S1381-1169(02)00126-7.

[44] D. Briggs, Handbook of X-Ray and Ultraviolet photoelectron spectroscopy, Heyden, 1977.

[45] N.S. McIntyre, D.G. Zetaruk, X-ray photoelectron spectroscopic studies of iron oxides, Anal. Chem. 49 (1977) 1521–1529, https://doi.org/10.1021/ac50019a016.

[46] A.P. Grosvenor, B.A. Kobe, M.C. Biesinger, N.S. McIntyre, Investigation of multiplet splitting of Fe 2p XPS spectra and bonding in iron compounds, Surf. Interface Anal. 36 (2004) 1564–1574, https://doi.org/10.1002/sia.1984.

[47] D.J. Young, High temperature oxidation and corrosion of metals, Elsevier, 2008.

[48] M.C. Biesinger, C. Brown, J.R. Mycroft, R.D. Davidson, N.S. McIntyre, X-ray photoelectron spectroscopy studies of chromium compounds, Surf. Interface Anal. 36 (2004) 1550–1563, https://doi.org/10.1002/sia.1983.

[49] M. Aronniemi, J. Sainio, J. Lahtinen, Chemical state quantification of iron and chromium oxides using XPS: The effect of the background subtraction method, Surf. Sci. 578 (2005) 108–123, https://doi.org/10.1016/j.susc.2005.01.019.

[50] T. Miyazawa, T. Terachi, S. Uchida, T. Satoh, T. Tsukada, Y. Satoh, Y. Wada, H. Hosokawa, Effect of hydrogen peroxide on corrosion of stainless steel, (V) characterization of oxide film with multilateral surface analyses, J. Nuclear Sci. Technol. 43 (2006) 884, https://doi.org/10.1080/18811248.2006.9711173.

[51] H.A. Smith, J.F. Fuzek, The adsorption of fatty acids on nickel and platinum catalysts, J. Am. Chem. Soc. 68 (1946) 229, https://doi.org/10.1021/ja01206a023.

[52] D. Barreca, G.A. Battiston, D. Berto, R. Gerbasi, E. Tondello, Chemical vapor deposited Fe_2O_3 thin films analyzed by XPS, Surf. Sci. Spectra 8 (2002) 240, https://doi.org/10.1116/11.20020302.

[53] M. Pyeon, T.-P. Ruoko, J. Leduc, Y. Gönüllü, M. Deo, N.V. Tkachenko, S. Mathur, Critical role and modification of surface states in hematite films for enhancing oxygen evolution activity, J. Mater. Res. 33 (2018) 455–466, https://doi.org/10.1557/jmr.2017.465.

[54] G.A. Attard, K. Chibane, H.D. Ebert, R. Parsons, The adsorption and decomposition of methanol on Pt(110), Rev. Sci. Instrum. 224 (1989) 311–326.

[55] G. Kataby, R. Prozorov, A. Gedanken, Characterization of self-assembled alcohols coatings on amorphous iron, Nanostruct. Mater. 12 (1999) 421–424, https://doi.org/10.1016/S0965-9773(99)00149-X.

[56] Y. Zhang, A. Savara, D.R. Mullins, Ambient-pressure XPS studies of reactions of alcohols on $SrTiO_3$ (100), J. Phys. Chem. C 121 (2017) 23436–23445, https://doi.org/10.1021/acs.jpcc.7b06319.

[57] G.P. López, D.G. Castner, B.D. Ratner, XPS O 1s binding energies for polymers containing hydroxyl, ether, ketone and ester groups, Surf. Interface Anal. 17 (1991) 267–272, https://doi.org/10.1002/sia.740170508.

[58] Z. Liu, T. Duchoň, H. Wang, D.C. Grinter, I. Waluyo, J. Zhou, Q. Liu, B. Jeong, E. J. Crumlin, V. Matolín, D.J. Stacchiola, J.A. Rodriguez, S.D. Senanayake, Ambient pressure XPS and IRRAS investigation of ethanol steam reforming on Ni-CeO_2(111) catalysts: an in situ study of C-C and O-H bond scission, PCCP 18 (2016) 16621–16628, https://doi.org/10.1039/C6CP01212D.

[59] E.T. Denisov, I.B. Afanasev, Oxidation and antioxidants in organic chemistry and biology, CRC Press (2005), https://doi.org/10.1201/9781420030853.

[60] W. Taifan, J.-F. Boily, J. Baltrusaitis, Surface chemistry of carbon dioxide revisited, Surf. Sci. Rep. 71 (2016) 595–671, https://doi.org/10.1016/j.surfrep.2016.09.001.

[61] J. Wielant, T. Hauffman, O. Blajiev, R. Hausbrand, H. Terryn, Influence of the iron oxide acid-base properties on the chemisorption of model epoxy compounds studied by XPS, J. Phys. Chem. C 111 (2007) 13177–13184, https://doi.org/10.1021/jp072354j.

[62] A. Glisenti, G. Favero, G. Granozzi, Reactivity of simple alcohols on Fe_2O_3 powders, an XPS and FTIR study, Faraday Trans. 94 (1998) 173–182, https://doi.org/10.1039/A705704K.

[63] J.M. Vohs, M.A. Barteau, Conversion of methanol, formaldehyde and formic acid on the polar faces of zinc oxide, Surf. Sci. 176 (1986) 91–114, https://doi.org/10.1016/0039-6028(86)90165-2.

[64] S. Tardio, M.-L. Abel, R.H. Carr, J.E. Castle, J.F. Watts, Comparative study of the native oxide on 316L stainless steel by XPS and ToF-SIMS, J. Vac. Sci. Technol. A 33 (2015) 05E122, https://doi.org/10.1116/1.4927319.

[65] C.-O.-A. Olsson, P. Agarwal, M. Frey, D. Landolt, An XPS study of the adsorption of organic inhibitors on mild steel surfaces, Corros. Sci. 42 (2000) 1197–1211, https://doi.org/10.1016/S0010-938X(99)00140-7.

[66] E. Johansson, L. Nyborg, XPS study of carboxylic acid layers on oxidized metals with reference to particulate materials, Surf. Interface Anal. 35 (2003) 375–381, https://doi.org/10.1002/sia.1537.

[67] P. Taheri, J. Wielant, T. Hauffman, J.R. Flores, F. Hannour, J.H.W. de Wit, J.M. C. Mol, H. Terryn, A comparison of the interfacial bonding properties of carboxylic acid functional groups on zinc and iron substrates, Electrochim. Acta 56 (2011) 1904–1911, https://doi.org/10.1016/j.electacta.2010.10.079.

[68] U. Gelius, P.F. Hedén, J. Hedman, B.J. Lindberg, R. Manne, R. Nordberg, C. Nordling, K. Siegbahn, Molecular spectroscopy by means of ESCA III, Carbon Compounds. Phys. Scr. 2 (1970) 70–80, https://doi.org/10.1088/0031-8949/2/1-2/014.

[69] G. Busca, IR study of isopropanol adsorption on haematite, React. Kinet. Catal. Lett. 20 (1982) 373–376, https://doi.org/10.1007/BF02066329.

[70] S.U. Yoon, B. Mahanty, H.M. Ha, C.G. Kim, Phenol adsorption on surface-functionalized iron oxide nanoparticles: modeling of the kinetics, isotherm, and

mechanism, J. Nanopart. Res. 18 (2016) 215, https://doi.org/10.1007/s11051-016-3478-y.
[71] U. Becker, M.F. Hochella, E. Apra, The electronic structure of hematite 001 surfaces; applications to the interpretation of STM images and heterogeneous surface reactions, Am. Mineral. 81 (11–12) (1996) 1301–1314, https://doi.org/10.2138/am-1996-11-1201.
[72] W. Hückel, Theoretical Principles of Organic Chemistry vol. II (1958) 435.
[73] E. McCafferty, A.C. Zettlemoyer, Adsorption of water vapour on α-Fe_2O_3, Discuss. Faraday Soc. 52 (1971) 239–254, https://doi.org/10.1039/DF9715200239.
[74] S. Lee, R.W. Staehle, Adsorption studies of water on copper, nickel, and iron using the quartz-crystal microbalance technique: Assessment of BET and FHH models of adsorption, Mater. Corros. 48 (2) (1997) 86–94, https://doi.org/10.1002/maco.19970480203.
[75] J. Frenkel, Kinetic Theory of Liquids, Oxford University Press, Oxford, 1946.
[76] Hill, T. L. (1952). *Theory of Physical Adsorption* (pp. 211–258). https://doi.org/10.1016/S0360-0564(08)60615-X.
[77] C.H. Giles, T.H. MacEwan, S.N. Nakhwa, D. Smith, 786. Studies in adsorption. Part XI. A system of classification of solution adsorption isotherms, and its use in diagnosis of adsorption mechanisms and in measurement of specific surface areas of solids, J. Chem. Soc. 3973 (1960), https://doi.org/10.1039/JR9600003973.
[78] G.M. Førland, K.J. Børve, H. Høiland, A. Skauge, Adsorption of short chain alcohols from decane solutions onto kaolinite, J. Colloid Interface Sci. 171 (1995) 261–269, https://doi.org/10.1006/jcis.1995.1179.
[79] R.E. Day, G.D. Parfitt, Adsorption at the solid-liquid interface. Part 4.—Adsorption of ethanol, n-octanol and n-dodecanol on defined rutile surfaces from binary liquid mixtures with p-xylene and n-heptane, Trans. Faraday Soc. 64 (1968) 815–822, https://doi.org/10.1039/TF9686400815.
[80] A. Tsugita, T. Takei, M. Chikazawa, T. Kanazawa, Phase transition in water adsorbed on .alpha.-ferric oxide surfaces, Langmuir 6 (9) (1990) 1461–1464, https://doi.org/10.1021/la00099a006.
[81] R.I. Slavchov, I.B. Ivanov, Adsorption parameters and phase behaviour of non-ionic surfactants at liquid interfaces, Soft Matter 13 (46) (2017) 8829–8848, https://doi.org/10.1039/C7SM01370A.
[82] P.R. Basford, W.D. Harkins, S.B. Twiss, Effect of Temperature on the Adsorption of n-Decane on Iron, J. Phys. Chem. 58 (4) (1954) 307–312, https://doi.org/10.1021/j150514a005.
[83] W. Weiss, W. Ranke, Surface chemistry and catalysis on well-defined epitaxial iron-oxide layers, Prog. Surf. Sci. 70 (2002) 1–151, https://doi.org/10.1016/S0079-6816(01)00056-9.
[84] N. Dzade, A. Roldan, N. de Leeuw, A density functional theory study of the adsorption of benzene on hematite (α-Fe_2O_3) surfaces, Minerals 4 (2014) 89–115, https://doi.org/10.3390/min4010089.
[85] J.S. Rowlinson, Liquids and liquid mixtures, London, Boston, Butterworth Scientific, 1982.
[86] T. Allen, R.M. Patel, Determination of specific surface using the flow microcalorimeter, Powder Technol. 2 (2) (1968) 111–120, https://doi.org/10.1016/0032-5910(68)80045-2.
[87] G.D. Parfitt, I.J. Wiltshire, Adsorption at the solid-liquid interface. II. Alcohols on rutile from solutions in p-xylene, J. Phys. Chem. 68 (1964) 3545–3549, https://doi.org/10.1021/j100794a018.
[88] R.E. Day, G.D. Parfitt, Factors involved in adsorption at the solid/liquid interface, Powder Technol. 1 (1967) 3–10, https://doi.org/10.1016/0032-5910(67)80002-0.
[89] B.A. Englin, A.F. Plate, V.M. Tugolukov, M.A. Pryanishnikova, Solubility of water in individual hydrocarbons, Chem. Technol. Fuels Oils 1 (1965) 722–726, https://doi.org/10.1007/BF00721855.
[90] A. Maączyński, M. Góral, B. Wiśniewska-Gocłowska, A. Skrzecz, D. Shaw, Mutual solubilities of water and alkanes, Monatshefte Für Chemie / Chemical Monthly 134 (2003) 633–653, https://doi.org/10.1007/s00706-002-0561-0.
[91] D.H. Everett, The thermodynamics of adsorption. Part II.—Thermodynamics of monolayers on solids, Trans. Faraday Soc. 46 (1950) 942–957, https://doi.org/10.1039/TF9504600942.
[92] H.A. Spikes, A. Cameron, Additive interference in dibenzyl disulfide extreme pressure lubrication, ASLE Trans. 17 (1974) 283–289, https://doi.org/10.1080/05698197408981467.
[93] Spikes H. A. Physical and chemical adsorption in boundary lubrication. Ph.D.: UK, 1972.
[94] B. Peychev, R.I. Slavchov, Adsorption model and phase transitions of diblock perfluoroalkylated surfactants at the water|alkane interface, J. Colloid Interface Sci. 594 (2021) 372–388, https://doi.org/10.1016/j.jcis.2021.02.057.
[95] R.I. Slavchov, I.M. Dimitrova, I.B. Ivanov, Cohesive and Non-cohesive Adsorption of Surfactants at Liquid Interfaces, in: R. Rubio (Ed.), Without Bounds: A Scientific Canvas of Nonlinearity and Complex Dynamics. Understanding Complex Systems, Springer, Berlin, Heidelberg, 2013, https://doi.org/10.1007/978-3-642-34070-3_22.
[96] Hadjiivanov, K. Identification and characterization of surface hydroxyl groups by infrared spectroscopy. In *Advances in Catalysis*; Jentoft, F. C., Ed.; Academic Press, 2014; Vols. 57, pp. 99–318. https://doi.org/10.1016/B978-0-12-800127-1.00002-3.
[97] G. Busca, V. Lorenzelli, IR characterization of surface hydroxy groups on haematite, React. Kinet. Catal. Lett. 15 (1980) 273.
[98] J.N. Israelachvili, Intermolecular and surface forces, third ed., Elsevier, 2011.
[99] Z. Szklarska-Smialowska, G. Wieczorek, Adsorption isotherms on mild steel in H_2SO_4 solutions for primary aliphatic compounds differing in length of the chain, Corrosion Sci. 11 (1971) 843, https://doi.org/10.1016/S0010-938X(71)80048-3.